NATIONAL AERONAUTICS AND SPACE ADMINISTRATION

Technical Memorandum 33-592

ATS-F Radiant Cooler Contamination Test in a Hydrazine Thruster Exhaust

Jose E. Chirivella

JET PROPULSION LABORATORY
CALIFORNIA INSTITUTE OF TECHNOLOGY
PASADENA, CALIFORNIA

April 15, 1973

TECHNICAL REPORT STANDARD TITLE PAGE

1. Report No. 33-592	2. Government Accession No.	3. Recipient's Catalog No.
4. Title and Subtitle ATS-F RADIANT COOLER CONTAMINATION TEST IN A HYDRAZINE THRUSTER EXHAUST		5. Report Date April 15, 1973 6. Performing Organization Code
7. Author(s) Jose E. Chirivella		8. Performing Organization Report No.
9. Performing Organization Name and Address JET PROPULSION LABORATORY California Institute of Technology 4800 Oak Grove Drive Pasadena, California 91103		10. Work Unit No. 11. Contract or Grant No. NAS 7-100 13. Type of Report and Period Covered Technical Memorandum
12. Sponsoring Agency Name and Address NATIONAL AERONAUTICS AND SPACE ADMINISTRATION Washington, D.C. 20546		14. Sponsoring Agency Code
15. Supplementary Notes		

16. Abstract

A test was conducted under simulated space conditions to determine the potential thermal degradation of the ATS-F radiant cooler from any contaminants generated by a 0.44-N (0.1-lbf) hydrazine thruster. The radiant cooler, a 0.44-N (0.1-lbf) hydrazine engine, and an aluminum plate simulating the satellite interface were assembled to simulate their flight configuration. The cooler was provided with platinum sensors for measuring temperature, and its surfaces were instrumented with six quartz crystal microbalance units (QCM) to measure contaminant mass deposits. The complete assembly was tested in the molecular sink vacuum facility (Molsink) at the Jet Propulsion Laboratory. This was the first time that a radiant cooler and a hydrazine engine were tested together in a very-high-vacuum space simulator, and this test was the first successful measurement of detectable deposits from hydrazine rocket engine plumes in a high vacuum. The engine was subjected to an accelerated duty cycle of 1 pulse/min, and after 2h of operation, the QCMs began to shift in frequency. The tests continued for several days and, although there was considerable activity in the QCMs, the cooler never experienced thermal degradation. Identification of the contaminants had not been completed at the time of this writing, but when the temperature of the radiant cooler surface is factored in (greater than 150 K) certain species

17. Key Words (Selected by Author(s))	18. Distribution Statement
Propulsion, Liquid Quality Assurance and Reliability Temperature Control Test Facilities and Equipment	Unclassified -- Unlimited

19. Security Classif. (of this report)	20. Security Classif. (of this page)	21. No. of Pages	22. Price
Unclassified	Unclassified	77	

TECHNICAL REPORT STANDARD TITLE PAGE

1. Report No. 33-592	2. Government Accession No.	3. Recipient's Catalog No.
4. Title and Subtitle		5. Report Date
		6. Performing Organization Code
7. Author(s)		8. Performing Organization Report No.
9. Performing Organization Name and Address JET PROPULSION LABORATORY California Institute of Technology 4800 Oak Grove Drive Pasadena, California 91103		10. Work Unit No. 11. Contract or Grant No. NAS 7-100 13. Type of Report and Period Covered
12. Sponsoring Agency Name and Address NATIONAL AERONAUTICS AND SPACE ADMINISTRATION Washington, D.C. 20546		14. Sponsoring Agency Code

15. Supplementary Notes

16. Abstract

of gases are immediately eliminated from consideration. Included among the remaining candidates are water, unreacted hydrazine, and ammonium hydrates.

17. Key Words (Selected by Author(s))	18. Distribution Statement		
19. Security Classif. (of this report)	20. Security Classif. (of this page)	21. No. of Pages	22. Price

NATIONAL AERONAUTICS AND SPACE ADMINISTRATION

Technical Memorandum 33-592

ATS-F Radiant Cooler Contamination Test in a Hydrazine Thruster Exhaust

Jose E. Chirivella

JET PROPULSION LABORATORY
CALIFORNIA INSTITUTE OF TECHNOLOGY
PASADENA, CALIFORNIA

April 15, 1973

PREFACE

The work described in this report was performed by the Propulsion Division of the Jet Propulsion Laboratory.

ACKNOWLEDGMENT

The author would like to acknowledge the cooperation of the International Telephone and Telegraph Corporation for providing the radiant cooler assembly and, along with the NASA Goddard Space Flight Center, for freely discussing all applicable technical areas. Furthermore, the author acknowledges the continuous assistance and dedication of the following individuals: J. Lee, for setting up and installing the test hardware; P. I. Moynihan, for the propellant feed module and for the discussion and revision of the manuscript; C. Zachman, for his original ideas and delicate handling of the quartz crystal microbalance instrumentation; and J. B. Stephens, for his contributions in the actual Molsink operations and in the discussion of the results.

CONTENTS

CONTENTS (contd)

TABLES (contd)

FIGURES

FIGURES (contd)

FIGURES (contd)

FIGURES (contd)

ABSTRACT

A test was conducted under simulated space conditions to determine the potential thermal degradation of the ATS-F radiant cooler from any contaminants generated by a 0.44-N (0.1-lbf) hydrazine thruster. The radiant cooler, a 0.44-N (0.1-lbf) hydrazine engine, and an aluminum plate simulating the satellite interface were assembled to simulate their flight configuration. The cooler was provided with platinum sensors for measuring temperature, and its surfaces were instrumented with six quartz crystal microbalance units (QCM) to measure contaminant mass deposits. The complete assembly was tested in the molecular sink vacuum facility (Molsink) at the Jet Propulsion Laboratory. This was the first time that a radiant cooler and a hydrazine engine were tested together in a very-high-vacuum space simulator, and this test was the first successful measurement of detectable deposits from hydrazine rocket engine plumes in a high vacuum. The engine was subjected to an accelerated duty cycle of 1 pulse/min, and after 2h of operation, the QCMs began to shift in frequency. The tests continued for several days and, although there was considerable activity in the QCMs, the cooler never experienced thermal degradation. Identification of the contaminants had not been completed at the time of this writing, but when the temperature of the radiant cooler surface is factored in (greater than 150 K) certain species of gases are immediately eliminated from consideration. Included among the remaining candidates are water, unreacted hydrazine, and ammonium hydrates.

I. INTRODUCTION AND SUMMARY

As a result of trends toward lower-thrust monopropellant engines and an increase of sophistication in spacecraft instrumentation, there is a growing interest in the effects that the thruster effluent may have on sensitive surfaces. For unmanned missions, the rocket exhaust materials could account for most of the rarified "cloud" that surrounds the spacecraft. The exhaust products from the attitude propulsion subsystem (APS) are of specific interest because of thrusters located at various points on the spacecraft. The APS engines are fired at frequent, discrete intervals throughout an entire mission, and some sensitive areas of the spacecraft are unavoidably immersed in their plumes.

Different satellites have experienced anomalies (e.g., USAF Model 35, NASA Nimbus II and III) that may have been caused by plume impingement effects. These questions have led the NASA Goddard Space Flight Center (GSFC) to assess the effect of the possible APS plume contamination of an infrared sensor radiant cooler. A cooler of this design is to be installed aboard the ATS-F satellite and located in the proximity of a small APS hydrazine thruster. A potential thermal degradation of the cooler could be caused by contaminant deposits on the low-emissivity surface of the cooler's first stage. The physics of such a process is very difficult to model theoretically at the present state of the art, and therefore a space simulation experiment was envisioned that could, within certain restrictions, provide information relevant to the behavior of the cooler in flight.

Considering the fact that both space radiation and a high vacuum environment must be simulated, a very special space simulator with a negligible recirculation effect had to be used for such a test.

The JPL Molecular Sink Facility (Molsink), for reasons to be described later, was selected. The radiant cooler, along with an aluminum plate simulating the spacecraft interface and a 0.44-N (0.1-lbf) hydrazine engine, were assembled to approximate the flight configuration. The radiant cooler was provided with platinum sensors for measuring temperature, and its surface was instrumented with six quartz crystal microbalance (QCM) units. A QCM is essentially an oscillator for which the resonance frequency is controlled by the piezoelectric effect of a quartz crystal. Under certain conditions, one can design the oscillator such that the frequency depends only on the mass of the crystal (including surface deposits), thus providing a means of measuring very small mass deposits.

The entire assembly was tested inside the Molsink, this being the first time that a radiant cooler and a hydrazine engine were tested together in a high-vacuum simulator. The engine was subjected to an accelerated duty cycle of 1 pulse/min, and after 2 h of operation, the QCMs began to shift in frequency, indicating that they were sensing mass deposits. The test continued for several days and, although there was considerable QCM activity, the cooler never experienced thermal degradation.

Although complete identification of the contaminants was not determined, when the crystal surface temperature was considered (greater than 150 K), species of gases with lower condensation points were immediately eliminated. Included among the remaining candidates are water, unreacted hydrazine, ammonium hydrates, and methane. This test was the first successful measurement of detectable deposits from hydrazine rocket engine plumes in high vacuum.

II. OBJECTIVES

The objectives of the experiment were:

(1) To determine whether the hydrazine thruster exhaust products will contaminate the cooler surfaces and cause the cooler to warm up.

(2) To determine, if the cooler does warm up, whether the stage heaters can remove the contamination by evaporation and restore the cooler to its normal temperature.

(3) To determine the anticipated heater duty cycle (if required for evaporation of contaminants) for the ATS-F thruster duty cycle.

(4) To determine the amount of exhaust products condensing on the cooler per thruster firing and the equivalent cooler temperature rise for the first firing duty cycle that shows degradation on cooler performance.

(5) To force contamination of the cooler with a jet of steam situated so as to "guarantee cooler contamination" and to observe the cooler response.

III. MOLSINK FACILITY

For a proper evaluation of the experiment and a deeper insight into the discussion of results, a general understanding of the Molsink facility and its working principles is necessary. The Molsink is an ultrahigh-vacuum facility which consists of three concentric chambers (see Fig. 1a). The innermost chamber is a sphere approximately 3 m (10 ft) in diameter, maintained at a temperature between 10 and 15 K with gaseous helium. The aluminum Moltrap walls are wedge-shaped, resembling an anechoic chamber, with a total surface area of approximately 186 m^2 (2000 ft^2) (see Fig. 1b). The chamber walls are also coated with titanium, which acts as a "getter" material to trap helium and hydrogen that are not cryopumped by the 10 K surfaces. The amount of helium and hydrogen that can be pumped is greatly increased by coating the walls with a frost of a gas that has a relatively high melting point. Under this condition, the frost cryosorbs helium and hydrogen at a very high rate. Carbon dioxide has been used routinely for such purposes in Molsink operations. Since, in general, only a molecular layer of hydrogen is cryosorbed by a frost molecular layer, a continuous bleeding of carbon dioxide is necessary if hydrogen is being periodically injected into the vacuum chamber.

The behavior of a rocket plume in the Molsink can be described by comparing the flow field both in space and inside the chamber (see Figs. 2a

and 2b). The rocket exhaust in space expands freely in an almost radial flow (Fig. 2a). If a hypothetical perfect sink surface enclosed such a plume (Fig. 2b), the flow field enclosed by such a surface would be identical to one experienced in space. This is the working principle of the Molsink chamber. However, since the walls of the chamber are not perfect sinks, a small molecular reflection occurs. This reflection results in a recirculation effect that could degrade the space simulation if the reflection coefficient were allowed to grow. The molecular trapping is very effective for gases other than hydrogen and helium. For these two gases, the cryosorption rate is highly dependent on the wall temperature, and therefore any process that affects the wall temperature will result in a variation of the chamber background pressure once hydrogen has been injected into the chamber.

During Molsink testing operations, a cryogenic environment exists inside the chamber. In order to operate the hardware inside the chamber, thermal control is necessary for items such as propellant lines and valves that are sensitive to freezing. These warm surfaces are protected from radiation cooling losses by appropriate shielding, and the heat conduction losses are negligible if low pressure is maintained inside the chamber. If, for some reason, the hydrogen sorption onto the wall is diminished, any additional hydrogen injected into the chamber will reduce the vacuum, resulting in an increase in heat conduction losses. This causes an additional warming of the walls, which results in more hydrogen desorption. This phenomenon has an exponential growth and results in the rapid desorption of hydrogen from the walls occurring within a matter of seconds; it will be referred to hereafter as the "avalanche effect."

The Molsink has two doors. The upper door is used as a feedthrough for the propulsion system lines and thermal controls. The signal lines from the various sensors inside the chamber are fed through the lower door. The bottom door temperature was maintained around 100 K. Special cautions are necessary for experiments where cold space simulation is required. For the particular tests involved in this effort, an aluminum foil was placed about 71 cm (28 in.) above the doors. The foil, with its top side sprayed with a low-outgassing black paint, was clamped at the lower part of the molecular trap. In this manner, two cavities were radiatively decoupled, one at 10 K (cold space) and the other (the space between the aluminum foil and the lower

door) at 100 K. For a general perspective of the way the systems were arranged inside the chamber, see Fig. 3. Greater details on this figure will be given in a later section, and more information about the Molsink facility can be found in Refs. 1-3.

IV. PROPULSION SYSTEM

A. Simulation of Engine Conditions

In order to more closely simulate the actual ATS-F flight conditions and still accomplish the test in a timely and expeditious manner, a Rocket Research 0.44-N (0.1-lbf) thruster/valve assembly that had been purchased for an earlier JPL test program was made available for this experiment. The thruster, Rocket Research MR-74, S/N 02, has the characteristics listed in Table 1. The valve is a Moog in-line solenoid with a soft (Teflon) seat. Its characteristics are presented in Table 2. Flow control was accomplished by an all-titanium, three-stage Lee Company Viscojet. (A Viscojet is typically available with one to five stages, depending on the required pressure drop, ΔP).

Since the thruster had been obtained for an earlier test program, it had already undergone a limited test series prior to its committal to the Molsink. The thruster/valve assembly had been subjected to a complete Thermoelectric Outer Planets Spacecraft (TOPS) vibration duty cycle (similar to a Mariner-Mars 1971 duty cycle), which includes a simulation of launch conditions. In addition to the vibration tests, it had also experienced 100,000 starts at an average initial temperature of 110°C (230°F) with approximately 0.01 second on-time. Therefore, at the time of the Molsink tests, the thruster was more representative of one that had been launched aboard a spacecraft, had executed reference acquisition, and had operated for some time in the limit cycle mode.

B. Subsystems

The engine and the valve were instrumented with several thermocouples and a coiled electrical heater. With this arrangement, thermal control of the engine catalytic bed could be maintained, while temperature readings of the throat, chamber, and other locations of interest on the

thruster/valve assembly could be obtained. A view of the engine, valve, Viscojet, and their instrumentation in an early phase can be seen in Fig. 4. A schematic diagram of the portions of the propulsion subsystem that were located inside the chamber is shown in Fig. 5. The fuel was introduced through Valve VF3, filling both lines with hydrazine from the solenoid valve to the check valve. The line containing the valve VN1 and the check valve was used as a gaseous nitrogen purge. Both the fuel and purge lines were packaged together with the carbon dioxide injection line (not shown in the figure) and shared the same thermal environment. This environment was controlled by a series of thermocouples distributed along the lines. The thermocouples controlled several low-outgassing Kapton film heaters manufactured by Electrofilm, Inc.[1] (see Figs. 6 and 7). The same type of heaters, as well as additional spot heaters, were used to thermally control the Viscojet/thruster/valve assembly described earlier (see Fig. 8).

The propulsion system was operated in a blowdown mode. The propellant feed module was located at the top of the Molsink chamber near the upper door (see Fig. 9), and the operations were commanded by remote control from the lower floor of the facility, after the propellant tank was pressurized. The remote controller, as well as the valve drivers and timer, is shown in Fig. 10. A schematic diagram of the propellant feed module, fuel and purge lines, and hydrazine valving system is given in Fig. 11. Details of the propulsion system operations are not presented in this report, but it should be emphasized that during the performance of a short off-time duty cycle, a small quantity of carbon dioxide must be injected into the chamber; hence a small, automatic injection system was devised to cope with the different engine duty cycles.

Although this was the first time that a monopropellant hydrazine thruster was fired in such a high vacuum simulator, all propulsion systems functioned nominally during the entire operation, and no further details are considered necessary for this report.

---

[1] 7116 Laurel Canyon Blvd., North Hollywood, California.

V. INSTRUMENTATION

One very important objective of the test was to monitor mass deposits on the sensitive surfaces of the radiant cooler. Since only traces of contaminants were expected, microbalance techniques were necessary for mass deposit detection. Quartz crystal microbalances (QCM) have been successfully used at JPL during the past several years. Because of the particular characteristics of this experiment, a special type of mounting and temperature compensation was adopted.

A. QCM Working Principles

A QCM consists of an electronic oscillator whose resonance frequency is stabilized by the piezoelectric effect of a quartz crystal. The resulting resonance frequency depends on several parameters, but if one fixes the oscillator circuit constants and polarization voltages, the specific modes of crystal vibration will depend only on the orientation of the cut plate with respect to the crystal axes. For QCMs, the AT cut is used, which yields, among others, a thickness vibration resonant mode of about 5 MHz. Depending on the angle of the AT cut, the precise resonance frequencies will depend both on the mass deposited on the surface of the crystal and the temperature. If the crystal experiences a variation in temperature ΔT and a mass variation ΔM, the frequency shift can be expressed as

$$\Delta f = C_M \Delta M + C_T \Delta T$$

where C_M and C_T are the mass coefficient and temperature coefficient of the crystal, respectively.

In general, C_M and C_T depend on the temperature and cut angles of the crystals. If a cut angle is chosen such that $C_T = 0$ for some range of temperature, the $\Delta f = C_M \Delta M$ and the crystal can be used as a delicate microbalance to detect and measure small masses deposited on the surface. It turns out that for a considerable change in temperature and cut angle, the mass coefficient does not vary more than 5%, and one can use the expression

$$\Delta M = \frac{\Delta f}{F_c^2} 4.30 \times 10^{-7}$$

for all practical purposes, where ΔM = mass deposits in g/cm^2, Δf = frequency shift in Hz, and F_c = resonant frequency in MHz.

An illustration of the crystal, along with the location of one of the electrodes and the thickness vibration mode, can be seen in Fig. 12. For an elementary treatment of the crystal oscillators, as well as crystal nomenclature, one can consult any standard electronics textbook (Ref. 4). An accounting of microbalance applications can be found in Refs. 5-11.

B. Temperature Compensation

As indicated in the last paragraph, in order to correlate the mass deposits with the frequency shift, it is necessary to select a crystal cut that makes $C_T = 0$ for the anticipated temperature variation range. Although this is obtainable for some applications, in most cases the frequency spectrum of the crystal becomes so complicated that the interpretation of the readings is very difficult, if not confusing. Bartera (Ref. 12) has designed a particular arrangement that within its simplicity provides a very efficient temperature compensation (see Fig. 13).

Consider two crystals, No. 1 and No. 2, both exposed to mass deposit and temperature variation. The corresponding change in frequency can be written as

$$\left.\begin{aligned} \Delta f_1 &= C_{M_1}\Delta M_1 + C_{T_1}\Delta T_1 \\ \Delta f_2 &= C_{M_2}\Delta M_2 + C_{T_2}\Delta T_2 \end{aligned}\right\} \qquad (1)$$

If both crystals have identical piezoelectric properties and are kept at the same temperature, then

$$C_{M_1} = C_{M_2},\ C_{T_1} = C_{T_2},\ \text{and}\ \Delta T_1 = \Delta T_2 \qquad (2)$$

Subtracting Eqs. (1) and taking Eqs. (2) into account, we have

$$\Delta F = \Delta f_1 - \Delta f_2 = C_{M_1}(\Delta M_1 - \Delta M_2)$$

and if one of the crystals is protected from mass deposits in such a way that $\Delta M_2 = 0$, we then have

$$\Delta F = C_{M_1} \Delta M_1$$

that is, the beat frequency shift ΔF of both crystals can be easily correlated with the mass deposits on one of them. For the conditions just described where $T_1 = T_2$, identical piezoelectric constants and $\Delta M_2 = 0$ can be achieved if one adopts the arrangement described in Fig. 13. A doublet crystal plate is cut and polished. Gold electrodes are deposited on one side, in the form indicated by the figure, while a rectangular electrode which is common to both parts of the doublet is used on the other side. Under these conditions, and if one drives the crystals at a low voltage, one can have two independent crystal oscillators. By protecting one of them from mass deposit with a screen that is optically thin to the environment radiation, the beat frequency shift of both crystals can be expressed as

$$\Delta F = C_{M_1} \Delta M_1$$

as was desired.

VI. THE ATS-F RADIANT COOLER AND ITS THERMAL AND QCM INSTRUMENTATION

The ATS-F cooler is a two-stage, rectangular cone with a sun shield (see Fig. 14). Its purpose is to cool an infrared semiconductor sensor to 100 K and maintain this temperature for the life of the experiment. The cooler's first stage is an asymmetric cone with a high-emissivity radiator located at the apex of the sun shield. The second stage, or "cold patch," is a rectangular radiator located at the apex of the first-stage cone. The second stage is isolated from the warm surroundings by the low-emissivity cone in the front and by a low-emissivity cold surface in the rear, radiatively coupled to a similar first-stage surface. The high-emissivity front surface radiating to cold space cools the second stage to roughly 100 K,

while the first stage radiator cools that stage to about 170 K. Any contamination which interferes with the radiative properties of any of the surfaces mentioned can change the radiative coupling between the stages or their surroundings and will cause the cooler to increase in temperature.

The cooler is provided with two heaters. One is located on the cold patch, while the other is on the first-stage surface. If contamination should cause the cooler to warm up, the heater output would be increased with the intent of evaporating the contaminants to restore the cooler surface to normal temperatures once the heaters were turned off. The surfaces of the cooler are provided with three platinum sensors. One is installed on the cold patch, a second is located on the first-stage cone near the first-stage radiator, while a third is on the same cone but near the cold patch.

Calibration tables of the platinum temperature sensors were available from the manufacturer, and readings of the resistances were performed by the circuits depicted in Fig. 15. The terminals of the sensors were brought out of the chamber and connected in series. A resistor of 100 kΩ was connected in series with the three sensors and a constant-voltage source. In this manner the resistance of sensor i was determined by $R_i = (V_i/V)R$.

Except for the presence of the molecular cold trap, the cooler had to have minimal obstructions in the field of view. This was the reason for covering the bottom door with the aluminum foil, as described earlier. This constraint forced the development of a delicate, miniature QCM mounting for the flat surfaces.

Six temperature-compensated QCM units were mounted on the cooler. Each QCM unit consisted of a doublet,[2] as described in Section V, two oscillators, and one mixer. The entire electronics package was condensed into a commercially available chip[3] and a schematic diagram of the circuitry can be seen in Fig. 16. The chip was small enough to be hidden under the crystal. Both the chip and the crystal were mounted with silver epoxy on

---

[2]Monitor Products, 815 Fremont Ave., South Pasadena, California.

[3]Celesco Industry, 3333 Harbor Blvd., Costa Mesa, California.

an elastic and thermally conductive structure. With this installation the thermal stresses were absorbed, and a good isothermal conductivity was established between the crystal and the cooler surfaces.

Details of the assembled unit without the wiring or mass shielding can be seen in Fig. 17a, where a unit is mounted on the mirror surface of the sun shield. The reflection on the mirror provides a view of the lower side. Another view of a different unit mounted on the first-stage radiator, along with a transparent Mylar mass shield and some wiring, is seen in Figs. 17b and 17c. Since the wiring is so extremely thin, the surface of the cooler is perturbed only slightly with this specific arrangement. The crystal locations and identifications in the cooler, as well as a general schematic diagram of the tested package, can be seen in Fig. 18. Three of the QCM units were mounted in the first-stage radiator, and three more in the inner side of the sun shield.

The mirror surface of the sun shield is aluminum, and in order to imitate the sticking coefficient, the exposed part of the doublet was coated with aluminum by a process of vacuum aluminum vapor deposition. Each QCM ground was kept floating and terminated outside the chamber. All cooler wiring was collected in a bundle, which was wrapped with several layers of Mylar and attached to the shroud walls through a Teflon bracket. In this manner, the heat leak from the cooler to the Molsink walls would be minimal.

Details of the wiring and QCM locations can be seen in Figs. 19a and 19b. One of the unknowns of the experiment was whether the radiant cooler would reach the nominal equilibrium temperatures after being perturbed by the QCM unit installations. Although not shown in the figures, the grounds from the QCM units installed on the first-stage radiator and later collected at the sun shield could act as a thermal path and cause the first stage to warm up. As will be seen later, this did not occur, and the entire unit experienced negligible thermal radiation perturbations.

VII. GENERAL ASSEMBLY OF THE PACKAGE

The radiant cooler, the thruster and satellite segment, and their relative positions in flight configuration, as depicted in Fig. 14, were

simulated at full scale by the arrangement shown in Fig. 18. The segment of the satellite that could have any effect on the thruster plume was mocked up to full scale by an aluminum plate and two aluminum panels. See Fig. 20a (front view) and Fig. 20b (mock-up rear). The cooler was suspended from the plate by four bolts. Each bolt was thermally controlled with a low-outgassing ceramic heater and a thermocouple, which would thus provide a thermal control of the housing, similar to the in-flight condition. A detail of the heater and its mounting on the plate, as well as on the control thermocouple, can be seen in Fig. 20c.

The whole package was inserted into the Molsink chamber and placed in a position such that the axis of the thruster and its plume coincided with the axis of the chamber. The plate was placed horizontally at approximately 2 m (6.6 ft) above the aluminum foil at the bottom of the chamber (see Fig. 3). The plate was suspended and fixed to the molecular trap by several thermally insulated turnbuckles. All the wiring and fuel lines, as well as most of the warm surfaces, were shielded with aluminized Mylar. Maximum thermal isolation was utilized for all components to minimize the heat leaks to the walls. Details of the general arrangement can be seen in the photographs in Figs. 21a and b and 22a and b. These photographs were taken shortly before closing the chamber.

VIII. TEST PROCEDURES

The system heaters were activated before the chamber was closed and evacuated. The facility is equipped with both a mechanical pump and a diffusion pump. The mechanical pump brings the vacuum to 1.33×10^{-1} N/m^2 (10^{-3} torr) and the diffusion pump continues it to 1.33×10^{-3} N/m^2 (10^{-5} torr) during nominal operations. The systems were maintained for 1 day with the heaters on and the chamber at 1.33×10^{-2} N/m^2 (10^{-4} torr) and room temperature. A small amount of gaseous nitrogen was continuously bled into the chamber, providing the systems with a 24 h baking period and a continual purging of the corresponding outgassing. At the end of that period, liquid nitrogen was introduced into the inner liner of the chamber; this brought the temperature of the inner liner and molecular trap to 80 K at the end of another 24 h. The pumps and the gaseous nitrogen bleeding were still

in progress. The vacuum pressure was 1.33×10^{-3} N/m^2 (10^{-5} torr). By this time, the systems had been outgassed for 48 h, and the helium system was turned on. The gaseous nitrogen injections were stopped. The chamber then reached 10 K and 1.33×10^{-7} N/m^2 (10^{-9} torr) pressure at the end of 8 h. At this point, the system heaters were set at nominal temperatures, as shown in Table 3, and the cooler heaters were turned off. Details of the test itself are described in Section IX.

IX. RESULTS

A. Data Acquisition System

1. DC signals. Signals from the thermocouples and the platinum sensors were fed into a cross-bar switch and then into a digital voltmeter (DVM). The digitized signal then entered a Hewlett-Packard Data Acquisition System.

2. AC signals. The signal was input into an RF relay which is controlled by the same cross-bar switch used for the dc signals, and the actual readings were made with a fixed delay to avoid the noise from the relay closure. The signal was cleaned by a low-pass filter, and then digitized by a programmable counter. Once the signal was digitized, it was fed into the data systems in the same manner as were the digitized dc signals.

B. Log of Operations

Data from all the thermocouples are available, but only the readings from the cooler thermal sensors and the QCMs will be shown. The data will be presented by calendar days overlapping for 8 h, i.e., from 0000 h to 0800 h of the following day.

The QCM output has been arranged in such a manner that a decrease in beat frequency corresponds to mass deposit on the crystal. The frequency shift is expressed in Hz and an approximate equivalence between Hz and molecular layers for several frosts is given in Table 4. The table has been constructed by assuming a 0.3-nm (3Å) separation between molecules and applying the equation for ΔM given in Section V-A.

August 11, 1972. The chamber was closed. The system heaters were activated and the mechanical pump started at 1400 h. The diffusion pump was operated at 1530, and at the same time liquid nitrogen was introduced into the inner liner, initiating the chilldown of the chamber. A small amount of gaseous nitrogen was being used continuously for purging purposes.

August 12, 1972. The systems were maintained at the same settings as the day before. The temperature of the chamber walls was down to 80 K, and the pressure of the chamber reached and was maintained at 1.33×10^{-2} N/m^2 (10^{-4} torr). A record of the radiant cooler temperatures can be seen in Fig. 23, although the cold patch temperature is not shown because of being out of calibration range. Readings on the cooler and the QCMs were not taken beyond 2100 h.

August 13, 1972. The heaters on the radiant cooler were turned off at 1400 h, and the system heaters were put under dynamic temperature control to maintain nominal temperatures (see Table 3). The helium refrigerator was started at 1415 h and the cooler temperature was recorded at the intervals indicated in Fig. 24.

August 14, 1972. The Molsink walls reached about 10 K at approximately 0100 h. The record of the ATS-F cooler temperatures is given in Fig. 25. The remaining systems were kept at steady state, while the Molsink background pressure was maintained less than 1.33×10^{-7} N/m^2 (10^{-9} torr). The QCM readings can be seen in Figs. 26a and 26b, although some uncertainties pertaining to the signals observed from the radiant cooler QCMs are suspected of being attributable to noise, so much so that the signal of Crystal 6 is not shown because of the difficulty in reading it.

August 15, 1972. The thermal control of the propellant lines and the carbon dioxide injection system was verified at 1100 h. The propulsion system was ready for the priming operation which began at 1450 h. The gaseous nitrogen present in the lines from the solenoid valve to the Molsink chamber feed-throughs was evacuated through the thruster by cycling the thruster valve. Because of the required in-place installations, the lines from the chamber feed-throughs to the propellant tank were filled with air. They were evacuated at approximately 1600 h, and a bigger rise in pressure was observed by the vacuum ionization gauge as the residual hydrazine vapors flowed through the thruster catalytic bed.

After a few minutes of Molsink vacuum in the fuel lines, the thruster valve was closed and the priming operation was begun by pressurizing the propulsion system and opening the propellant tank to approximately 2.4×10^5 N/m^2 (35 psia) and opening the propellant isolation valve. The thruster valve was operated several times, both manually and automatically, to ensure a hard prime. After several pulses, the propellant tank pressure was increased to 2.7×10^6 N/m^2 (400 psia), which was required to generate the 0.44-N (0.1-lbf) thrust. The thruster valve was then subjected to a series of pulses which, because of the presence of hydrogen, caused an increase in the Molsink pressure. The original vacuum was promptly recovered by injecting carbon dioxide. Nevertheless, and because of the residual hydrogen present in the chamber, the background pressure remained about 1.33×10^{-5} N/m^2 (10^{-7} torr) for most of the experiment. At 1845 h, the pulsing was stopped and the system was secured. About 20 pulses occurred during the priming operation.

The recordings of the radiant cooler temperatures are depicted in Fig. 27 and the sun shield QCM readings in Fig. 28. The cooler first-stage QCM readings are not shown because of a noisy signal modulation developed at the low-pass filter. One can see that the cooler experienced some thermal perturbation during the priming operation and that the surface temperatures were stabilized to within a couple of degrees after priming was terminated. The QCMs on the sun shield were still outgassing slightly and/or accepting mass before the priming. A considerable mass deposit and evaporation took place during priming for a short period of time. However, at the end of the operation, the QCMs were stabilized at a frequency slightly less than before, primarily for crystals 3 and 5. The other QCMs are not shown; but in spite of the noisy signals, one could observe a definite mass deposit during priming.

August 16, 1972. The systems were maintained at steady state until 1020 h. At that time the thruster was activated, and it was fired at a rate of one 200-ms pulse every minute. For this duty cycle, the temperature of the thruster shifted from 149°C (300°F) to 371°C (700°F), about which it stabilized. The radiant cooler temperature can be seen in Fig. 29 and the QCM readings in Figs. 30a and b. The signals of QCMs 4 and 6 are not

shown. The output from QCM 2 was acquired by a redundant data system consisting of a counter and a strip recorder. One can see that the crystal accepted a significant amount of mass. Two of the crystals on the sun shield reacted to the thruster operation almost instantly. The other on the sun shield and the one on the cooler took about 2 h to indicate any mass acceptance. To the best of our knowledge, the discrete variations of frequency observed in the figures are not correlated with any Molsink operation. The decrease in cooler temperature after the thruster was started will be discussed later.

During thruster operation, injections of small amounts of carbon dioxide were necessary to maintain the chamber background pressure around 1.33×10^{-4} N/m^2 (10^{-6} torr). The thruster was shut off around 2230 h; by that time, it had undergone about 790 pulses. About 30 min after the thruster operation was discontinued, the sun shield crystals altered their output pattern. Some mass evaporated from some of them while others maintained a steady signal output.

August 17, 1972. The cooler temperatures and all of the QCM readings were recorded on a redundant data system (see Figs. 31 and 32a and b). The thruster began firing at 0835 h, at a duty cycle of one 200-ms pulse per minute. At 1155 h, it was shut off to stabilize the background pressure from 5.0×10^{-3} N/m^2 (4×10^{-6} torr) to 1.4×10^{-3} N/m^2 (1.2×10^{-6} torr). An automatic carbon dioxide injection system was installed, and the thruster was restarted at 1256 h. At 1441 h, the thruster was shut off to adjust a malfunction of the carbon dioxide injection system. At 1526 h, the thruster was reactivated at the same duty cycle.

At 1802 h, an avalanche of hydrogen outgassing from the chamber wall took place, caused by a deficiency in carbon dioxide cryosorption. The helium refrigerator was stopped long enough for the hydrogen to be pumped out by the mechanical pump, after which it was restarted. At 1928 h, the chamber conditions were back to nominal and the thruster was restarted at the same duty cycle, where it remained at that setting until 2340 h, at which time the systems were turned off and secured to steady state. Note the increasing temperature of the radiant cooler caused by the increase in pressure of the chamber with the corresponding increase in thermal conductivity of the

background gases. Observe that during the hydrogen avalanche, the QCMs experienced a spike, but the output from the ones located on the sun shield are inverted with respect to that of the ones on the cooler. Note also that prior to the avalanche, the QCMs were detecting a slight mass deposit during thruster operation, although not so intense as the previous change. During this day, the thruster experienced 713 pulses.

August 18, 1972. The thruster began firing at 0858 h at a duty cycle of one 200-ms pulse every 2 min until 1307 h, at which time the duty cycle was restored to 1 pulse/min. At 2019 h, the thruster was shut off to allow carbon dioxide to cryosorb the excess hydrogen, and it was turned on again at 2100 h. Finally, it was stopped at 2309 h and the propulsion systems secured. During the entire operation, the temperature of the thruster was never less than 148.8°C (300°F).

Figures 33 and 34a and b show the radiant cooler temperatures and QCM readings for this day. A slight continuous mass deposit was observed in all the crystals. The sharp variations at 2330 h were observed because of an avalanche which was intentionally precipitated to desorb and evacuate hydrogen out of the chamber. The two slope variations of both the radiant cooler temperatures and QCM readings are caused by the cycling of the cooler heaters. During this day, the thrusters underwent 680 pulses. When the heaters were turned off, a mass deposit occurred almost instantaneously on the cooler crystals.

August 19, 1972. The thruster was set to operate at trains of 25 pulses of 200 ms spaced 10 s apart, which is the flight duty cycle. The spacing of the trains of pulses was arbitrarily set. The thruster was started at 1543 h, and 10 pulse trains were initiated. At 1800 h, the thruster was stopped and steam was injected through the bottom door several times. At 2100 h, the thruster was again operated at the new duty cycle. At 2347 h, the thruster was stopped and the system was secured.

Figures 35 and 36a and b show the radiant cooler temperatures and the QCM readings for this day. Observe that both the radiant cooler temperatures and the QCM outputs were still unaffected by the thruster operation. However, as a result of one of the steam injections, some of the sun shield crystals

accepted mass, although evaporation from the one that was worst affected occurred within 2 h. The crystals on the cooler did not absorb any mass, but rather one of them lost a discrete amount, possibly from erosion by the water pellets. At the end of the day, the thruster had undergone 625 more pulses.

August 20, 1972. The thruster was activated at 0900 h at a duty cycle of 12 trains of twenty-five 200-ms pulses spaced 10 s apart. At 1107 h, the thruster was stopped. At 1114 h, the cooler heaters were energized at 16 V. The voltage was increased to 25 V at 1423 h. At 1425 h, thermal control of the housing heaters was increased to 37.8°C (100°F), although this temperature was not reached for another 23 min. At 1527 h, the housing heaters were turned up to maximum output, but because of radiation losses, the temperature never exceeded 65.5°C (150°F).

At 2340 h, all the heaters on the radiant cooler and the housing were de-energized. The temperature readings and QCM outputs are depicted in Figs. 37 and 38a and b. It should be noted that the slopes of the radiant cooler QCM curves were very responsive to any manipulation of the cooler heaters, and the sun shield QCMs were very sensitive to the housing heater operations. Although a 10-min lag occurred, there was a marked response of all QCMs and platinum sensors to the OFF condition of the heaters. Signal 1 was lost from 2400 to 0800 of the next day, probably because of oscillator malfunctioning.

August 21, 1972. At 0900 h, the housing and the cooler heaters were turned on. At 1400 h, several bursts of steam were injected into the chamber as a safety measure to dilute any traces of hydrazine that may have been present in the chamber. At 1500 h, the refrigerator was turned off and the flow of liquid nitrogen into the inner liner was stopped. Readings of the cooler temperatures and QCMs were recorded and are displayed in Figs. 39 and 40a and b.

August 22, 1972. The vacuum pumping equipment to the chamber was turned off at 0830 h. At 1100 h, chamber purging with gaseous nitrogen was stopped and the chamber was left undisturbed for several hours. Figures 41 and 42a and b show the cooler temperatures and QCM readings.

August 23, 1972. The chamber back-filling began at 0800 h, and at approximately 1000 h, the system heaters were turned off. At this point the chamber was opened and the test terminated. Visual inspection of the QCMs indicated evidence of chemical attacks and changes in coloration, but at the time of this writing they had not been analyzed. The record of the radiant cooler temperatures is shown in Fig. 43.

X. ANALYSIS AND DISCUSSION OF RESULTS

A. Analysis

During the evacuation and chill-down of the Molsink chamber, a marked outgassing was experienced from all systems. Since outgassing rates vary as a function of the temperature and the nature of the materials, it is not unusual to find a relatively poor vacuum near some surfaces after several days of outgassing. Traces of outgassing, for example, can still be seen in Figs. 26a and b, as well as in the first 16 h of August 15, 1972 (Fig. 28). Nevertheless, the signals which Figs. 26a and b represent may also contain some noise from the low-pass filter, as mentioned in Section IX.

Care must be taken in the interpretation of the decay and stabilization of the radiant cooler temperature during setup operations. The evacuation with mechanical pumps and the liquid nitrogen chill-down to 80 K took place with the radiant cooler heaters on and with the housing warm. Only after 1400 h on August 13, 1972, with the housing temperature at 276 K, were the cooler heaters turned off. Although the helium refrigeration system was started 15 min later, the wall did not reach 10 K until 0100 h the following day. Thus, the exponential decay of the cooler temperatures observed between 1415 h and 0100 h in Fig. 24 is also caused by the Molsink wall cooling and does not simulate the condition that would exist in space. As can be seen, the cooler temperatures stabilized, in spite of the presence of the QCMs, to values that were sufficiently close to the predicted flight values to make the test meaningful.

All the systems were under automatic thermal control during the day of August 14, 1972, and the only activity in the chamber was the outgassing of the various systems. The chamber conditions remained relatively constant

until 1450 h, when the thruster priming operation began. The cooler temperature variations, as well as the outputs from the sun shield QCM units, present an interesting pattern worth analyzing. The temperatures of the first stage experienced a decrease of 3 °C, after the priming operations, while the cold patch temperature showed oscillations on the order of 1 K and a net decrease of about 1.5 °C after the priming was completed.

Since the opposite results should be expected, the only explanation that at present seems compatible with the physical constraints imposed on the hardware is the fact that the temperature of the sun shield was diminished by an increase in the heat conductance to the Molsink wall through the cooler and QCM instrumentation wiring. This increase in conductance could be caused by carbon dioxide frost deposits on the Teflon wiring insulation located at the chamber wall as shown in Fig. 22b (Points A and B). At low temperatures, the conductivity of the carbon dioxide frost is greater than that of Teflon, and, therefore, a higher heat leak could be expected. This could explain the net decrease in temperature of the cooler, but could not account for the cold patch temperature oscillations, since no such oscillations are observed in the first stage of the cooler.

This anomaly could possibly be caused by an increase in emissivity of the first-stage cone, resulting from the accretion and evaporation of some materials during the priming. The cooler QCM readings are not available for this day, but in Fig. 28 one can see considerable sun shield QCM activity during the priming interval. Assuming that the sun shield temperature was probably less than 0 °C (no thermal sensors were installed on the sun shield, but it is quite likely that it was running colder than the housing because of radiation losses and heat leaks through the wiring), and that the oscillations seen in the beat frequency of the crystals have periods of about 10-min duration, one can infer that at least two species of material were arriving at the crystal surfaces: one species with a high evaporation rate and the other with a slower rate. Note also that two of these crystals maintained some mass deposit after the priming was completed. A persistent noise masked the results of the radiant cooler QCMs, but the average signals shifted down by several hundred cycles, indicating mass deposits; however, the lack of reliability of the data systems for QCMs 2, 4, and 6 during this day prevents making any quantitative conjectures based on such data. The

oscillations in the cold patch temperature and the sun shield QCM frequency occurred after a delay of about 15 min from the beginning of engine priming, and more than 1 h after the gaseous nitrogen and air evacuation from the propulsion line.

During August 16, 1972, the sun shield QCMs 1 and 5 accepted mass as soon as the engine was turned on, as can be seen in Fig. 30a. On the other hand, the sun shield QCM 3 and the cooler QCM 2, which were geometrically close, as Fig. 18 shows, did not experience any mass deposits until approximately 3 h later (Figs. 30a and b).

This apparent anomaly is explainable by assuming the existence of two different molecular sources for the two groups of crystals. The origin of these two molecular sources could be speculated by several arguments and will be discussed later. The loss of the signals from QCMs 4 and 6 handicaps any detailed explanation of the peculiar QCM behavior. But, for the rest of the test, as seen from the radiant cooler QCM signals which were registered later, all three cooler QCMs behaved similarly. If one extrapolates these data, it appears possible that QCMs 4 and 6 have the same source of mass flux as QCMs 2 and 3.

After the engine was shut off, no variation was observed in the QCM signals during the first 30 min, but a sudden slope change took place in QCMs 1, 2, and 5 during the following hour: QCM 1 received a considerable amount of mass, with some subsequent evaporation, while QCM 5, which was more active during the early hours of the engine operation, at first showed a sharp mass acceptance, did not experience any mass evaporation, and stayed constant until the next day. During this period, QCM 3 experienced a smooth response curve; 2 h after the thruster was stopped, QCM 3 experienced a gentle but increasing evaporation. The QCM 2 on the cooler instantly lost a discrete mass, although it continued with the same mass-accepting rate for as long as 10 h.

The physical process involved in the propulsion system shut-down will not be covered in this report since it is not relevant to the results of this test program; however, there appears no doubt about the fact that the thruster operation and the QCM response were correlatable during this specific day. The cooler again experienced a decrease in temperature hours

after the thruster operation began. The carbon dioxide frost conductance explanation given earlier to account for the pseudo-increase in cooler performance could also be applied here. (A thick carbon dioxide frost bridged over the Teflon insulation could reduce the sun shield and/or housing temperature.) It should be noted that the temperature continued to decrease slightly but steadily for the remainder of that day and most of the next one (see Figs. 29 and 31).

The data obtained on August 17, 1972, does not indicate any significant temperature or QCM variation until the time that the hydrogen avalanche occurred. At that time, the hydrogen density increased and a rise in cooler surface temperatures, caused by the increase in gas conductivity between the housing and cooler, was experienced. The increase in cooler temperatures was accompanied by a desorption of the cooler QCMs that, when compared with the sorption of the sun shield QCMs, indicated a burst of hydrogen from the cooler along the housing and the sun shield.

It should be pointed out that the avalanche effect is a Molsink anomaly, and nothing of this nature would occur in space. Once the avalanche had ceased and the chamber background pressure was back down to 1.33×10^{-4} N/m^2 (10^{-6} torr), the radiant cooler temperatures began to go down again. The sun shield QCMs outgassed completely to the level at which they were before the avalanche, and the QCMs on the cooler followed the thermal pattern of the radiant cooler; i.e., they seemed to follow a thermal sorption-desorption cycle. However, the fact that they were sorbing during the cool-down indicated the existence of some frost that had not evaporated during the avalanche on the surface (see Figs. 31 and 32a and b). The discontinuity of QCM 1 at about 2200 h was caused by an intentional change in collector polarization voltage of the oscillator, and, therefore, it should be disregarded.

During the remainder of August 18, 1972, no effect of the thruster on the radiant cooler temperature or QCMs was observed. The cooler temperature stabilized at a value very close to the one that existed before the avalanche of the preceding day. The discrete jump in frequency of QCM 2 could be caused by loss of a particle. Since no subsequent frequency changes were observed, the thruster was stopped around 2300 h and an avalanche was intentionally triggered to pump the accumulated hydrogen. At 2400 h,

the pressure was back to 1.33×10^{-4} N/m^2 (10^{-6} torr), and the radiant cooler heaters were turned on. No effect from these heaters was observed on the sun shield QCM as expected. However, the radiant cooler temperatures and QCM followed the heater changes very closely. Figures 33, 34a, and 34b indicate that the cooler and sun shield instrumentation response followed the same pattern as during the previous avalanche. The behavior of the QCMs during the avalanche and the heater manipulations seemed to confirm the hypothesis of a thermal sorption and desorption cycle.

The same pattern was repeated the following day, August 19, 1972. The thruster was fired after the temperatures and QCMs were stabilized, but no effect was observed. The thruster was later shut off, after which several bursts of water vapor were directed toward the cooler from the bottom door. This had no effect (see Figs. 35, 36a and 36b) on the radiant cooler temperature. Other than QCM 2, which lost a discrete amount of mass (possibly by erosion), the cooler QCMs were not affected by the water injection either. The sun shield QCMs, however, were affected slightly by the water injection. The mass deposited on QCM 5 was slightly eroded; QCM 1 received some small amount of mass which remained for as long as 8 h. The QCM 3 accepted mass and lost it at two different rates. This behavior of QCM 3 was similar to the oscillations which occurred during the earlier priming operations, for which both a high and a low evaporation rate were observed (see Fig. 28).

By August 20, 1972, all instrumentation was well stabilized, and the thruster firing did not alter any of the signals, as can be seen by Figs. 37, 38a, and 38b. A decision to stop the thruster and attempt a last effort to evaporate whatever contaminants were on the QCM was made, and the cooler heaters were activated at 16 V. The platinum sensors and the QCMs reacted instantly to this perturbation but, as was anticipated, the sun shield QCMs remained undisturbed. A higher voltage (25 V) was applied to the radiant cooler heaters, and more power was supplied to the housing, which resulted in slope variations of the radiant cooler QCMs and outgassing of the sun shield QCMs. Later increases in housing heater voltage were reflected in slope changes for a sun shield QCM. All the heaters were turned off after 8 h of outgassing, and the entire set of QCMs started sorbing back

hydrogen mass, which required the existence of a sorbing substance that was not evaporated during the warming period.

The heaters were turned on again the following day, August 21, 1972, and the procedures for test termination began. One can see from the figures that the QCMs still followed the thermal desorption pattern, and that the water injection during this day affected some QCMs (Figs. 39, 40a, and 40b).

During August 22, 1972, the QCMs steadily lost mass as the chamber pressure and cooler and sun shield temperatures increased throughout the remainder of the day. After the refrigerator system was shut off (Figs. 39, 41, and 43), the cooler experienced a very slow warming rate to room temperature. This was primarily the result of the thermal superinsulation of the Molsink facility and the good isolation of the cooler from the Molsink walls. The radiant cooler QCMs followed the warming cycle as the temperatures were increased. The fact that the sun shield QCMs generally followed the same cycle implies that, assuming the validity of the QCM thermal sorption-desorption hypothesis, the sun shield was actually warming up and had remained colder than the anticipated 270 K during the tests.

B. Discussion

Several observations are inferred from the preceding analysis:

(1) The QCMs registered mass deposits. Temperature variations did not affect them directly because they were calibrated prior to the Molsink test from room temperature to liquid nitrogen temperature, and the frequency did not vary by more than three cycles per second over this entire temperature range.

(2) The hydrogen sorption and desorption masked the actual contaminant mass deposits. The only way to obtain a quantitative estimate of this effect would be to obtain a calibration as a function of temperature and sorbing material. Since this calibration would be expensive and lengthy, it was beyond the scope of this test. Thus, one must assume that the sorption/desorption process observed in the test was monomolecular. In other words, one molecular layer of hydrogen saturates the surface, and further sorption requires another frost-molecular layer.

(3) The cooler performance was not degraded, although some mass had been deposited. Nevertheless, the continuous conductive heat leak to the Molsink wall, and the fact that the sun shield was running cold, may have prevented such thermal degradation.

(4) The nature of the observed contaminants (deposits) is still uncertain. For the temperatures registered at the cooler, the gases carbon dioxide, hydrogen, nitrogen, and ammonia have very high evaporation rates. The water deposited on the QCMs during injection should have been evaporated after the many hours of radiant cooler warming, since even at 150 K, water sublimates at a fairly high rate (10^{-8} g/cm^2/s, or on the order of one molecular layer every second). The other alternative is that some unknown materials coming from the thruster or possibly from the outgassing of the entire test assembly were deposited on the QCMs. The frequency oscillations observed during priming and during the first hours of thruster operation appear to confirm that the source was indeed the thruster, since a point was reached where further frequency variation did not occur because of saturation of the frost layer and the lack of its mechanical coupling to the crystal vibrations.

Among the materials that could be discharged by the thruster as possible condensables are: water, methane, ammonium hydrates, or unreacted hydrazine. Water from the thruster would behave similarly to the water injected through the chamber door, and thus does not appear to be a good candidate because of its high evaporation rate at the temperatures concerned. Methane and also other hydrocarbons observed in this type of exhaust are probably the result of decomposition of aniline; they are quite volatile, but they could form persistent deposits. Moynihan (Ref. 13) as well as Brill and Stechman (Ref. 14) have found traces of unreacted hydrazine in steady state operations at 750°C. This situation could be aggravated if the engine were to run cooler 148°C (300°F), and in a transient (pulsed) mode in a very high vacuum. Thus, unreacted hydrazine is a reasonable candidate.

However, no vaporization rate data are available for hydrazine at the relatively low temperatures which existed during this test program.

(5) Since the plume has radial flow and the QCMs were shielded from any direct plume impingement, the only way to experience engine effluent material is by secondary, molecular emissions and/or by frost migration. This hypothesis seems to be confirmed by the delay in the response of the radiant cooler QCMs to thruster operations observed, and the prompt response of the sun shield QCMs during the first thruster operations. A conceptual model that could explain this indirect mass deposition is depicted in Fig. 44: a thin frost or liquid is deposited on the sun shield; when it reaches the rim it can either migrate into the cooler, or simply become a molecular source, and send material toward it.

XI. CONCLUSIONS

Considering the physical boundary conditions of the test, in addition to the results and their interpretations as discussed earlier, the following conclusions are offered:

(1) The QCM sensors functioned nominally and their readings were due only to mass either deposited or lost.

(2) The radiant cooler ran slightly warmer than nominal, but the presence of QCMs mounted on its surfaces did not cause this sensitive instrument to function significantly off the design conditions.

(3) The thruster operation did not thermally degrade the cooler. This fact could be due either to negligible contamination sources or to compensating conductive heat leaks from the cooler to the Molsink wall.

(4) The 5 °C temperature drop experienced by the cooler could be caused by an increased thermal conductivity of the cooler instrumentation wiring insulation as carbon dioxide and other frosts were formed on their surfaces.

(5) The radiant cooler heaters did not have enough power to evaporate the contaminants of the QCM surface. They were able to raise the cooler temperature only as high as 240 K.

(6) The sun shield of the cooler seems to play an important role in the mechanism of cooler contamination, although a proper evaluation of its significance cannot be assessed because of the absence of thermal instrumentation on its surface.

(7) The QCMs sensed contaminant mass deposition, but not in great quantities. The nature of the contaminants is not known, but many gases can be immediately discarded on the basis of high evaporation rates at the QCM temperatures. For example, at these test conditions, nitrogen, carbon dioxide, and ammonia would not condense. Among the remaining possibilities are water, unreacted hydrazine, and methane. Water and methane come from propellant impurities and they could be condensed on the cooler surfaces. However, they have high evaporation rates at 200 K and could not be present when the cooler heaters were turned on for 8 h. Unreacted hydrazine could come from the transients originating in the operation of the thruster at high vacuum. Very little is known about hydrazine's physical properties at low temperatures and pressures, and its evaporation rate at 200 K is not available. Another possibility is that the contaminants could originate as a result of outgassing of the various parts of the system. However, if that were the case, there would not be a correlation between the thruster firing and the QCM mass deposits during the first day.

(8) More testing is necessary to answer some of the questions encountered during this simulation, and to isolate the suspected sources of contaminants.

XII. RECOMMENDATIONS

The above conclusions have suggested the following recommendations:

(1) The tests should be repeated by installing additional instrumentation such as heaters and thermocouples on the sun shield. This would permit a thermal control of the sun shield.

(2) The conductive heat leak from the cooler to the Molsink wall could be intercepted by simply wrapping a strip heater with a thermocouple around the cooler instrumentation wiring. This would provide controllable opposing temperature gradients.

(3) The cooler should be provided with more powerful heaters to reach 300 K in a short period of time. This would reduce the warming-cooling cycle duration and would possibly evaporate the less volatile contaminants detected during the tests.

(4) The flight sun shield should be provided with thermal sensors and some form of heater. The modification would avoid the possibility of the sun shield running too cold and would discourage the migration and/or secondary molecular source emission of contaminants toward the cooler.

(5) The contaminants arrived at the cooler by some yet undetermined phenomenon. Further testing is therefore necessary to obtain a more realistic estimation of the possibility of experiencing the cooler's thermal degradation.

REFERENCES

1. Stephens, J. B., "Spacecraft Mechanism Testing in the Molsink Facility," in Proceedings of the 4th Aerospace Mechanisms Symposium, Technical Memorandum 33-425, edited by G. G. Herzl and M. F. Buehler, Jet Propulsion Laboratory, Pasadena, California, Jan. 15, 1970.

2. Stephens, J. B., "Molecular Sink," Research/Development, July 1967.

3. Stephens, J. B., "Space Molecular Sink Simulator Facility Design," Journal of Spacecraft and Rockets, June 1966.

4. Terman, E. F., Radio Engineers Handbook, McGraw-Hill Book Company, 1955.

5. Warner, A. W., "Micro Weighing With the Quartz Crystal Oscillator--Theory and Design," in Ultra Micro Weight Determination in Controlled Environments, edited by S. P. Wolsky and E. J. Zdanuk, Interscience Publishers, 1969.

6. Saurbrey, G. Z., Zeitschrift für Physik, Vol. 155, p. 206, 1959.

7. Stockbridge, C. D., Vacuum Microbalance Techniques, Vol. 5, pp. 193-205, 1965.

8. Eschbach, H. L., and Kruidhof, E. W., Vacuum Microbalance Techniques, Vol. 5, pp. 207-216, 1966.

9. Niedermayer, R., et al., Vacuum Microbalance Techniques, Vol. 5, pp. 217-229, 1966.

10. King, W. H., and Varga, G. M., Contract RC 9-439088 Final Report, Exxon Research Center, Linden, N. J., December 1969.

11. Crawford, H. M., et al., "The Design and Performance of the Piezoelectric Sorption Hygrometer," in Analysis and Instrumentation, Plenum Press, 1964.

12. Bartera, R. E., Quartz Crystal Oscillator Apparatus for Measuring Mass Accretion and Temperature Independently of Each Other, JPL Patent Case 11279, Jet Propulsion Laboratory, Pasadena, California.

13. Moynihan, P. I., Jet Propulsion Laboratory, Pasadena, California, private communication.

14. Brill, Y. C., Stechman, R. C., and Reiss, R. J., "Effect of Hydrazine Rocket Fuel on Spacecraft Materials," presented at the 14th Annual Technical Meeting of the Institute of Environmental Sciences, April 1968.

Table 1. Typical characteristics of Rocket Research 0.44-N (0.1-lbf) thruster (Model MR-74) used in this experiment

Parameter	Value
Steady state thrust level, N (lbf)	0.44 (0.1)
Steady state chamber pressure, N/cm^2 (psia)	223.0 (154.0)
Catalyst	Shell 405, 20-30 mesh
Nozzle expansion area ratio	71
Throat diameter, cm (in.)	0.0575 (0.02268)
Injector type	Flat face, Rigimesh screen
Steady state I_{sp}, N-s/Kg (lbf-s/lbm)	2075.0 (212.0)

Table 2. Typical characteristics of Moog in-line solenoid valve (P/N 010-58723-1) used in this experiment

Parameter	Value
Operating voltage, V dc	28.0
Pull-in voltage, V dc	10.5
Drop-out voltage dc	4.2
Opening response, ms	3.5
Closing response, ms	2.7
Internal leakage at 400 psig, standard cm^3 He/s	4.2×10^{-9}
Coil resistance, Ω	110.0

Table 3. Nominal temperatures of heaters

System	Temperature, °C
Fuel lines	20 - 30
Resistor jet	20 - 30
Solenoid valve	20 - 30
Catalytic bed	150
Thruster capillary inlet tube	20 - 30
Housing heaters	3

Table 4. Frequency mass equivalence

F_c = 5 Mz (approximate resonance frequency of single crystal)

Gas	X
H_2	4
N_2	0.52
NH_3	1.21
CO_2	0.50
H_2O	1.23
N_2H_4	2.80

1 Hz equals X molecular layers.

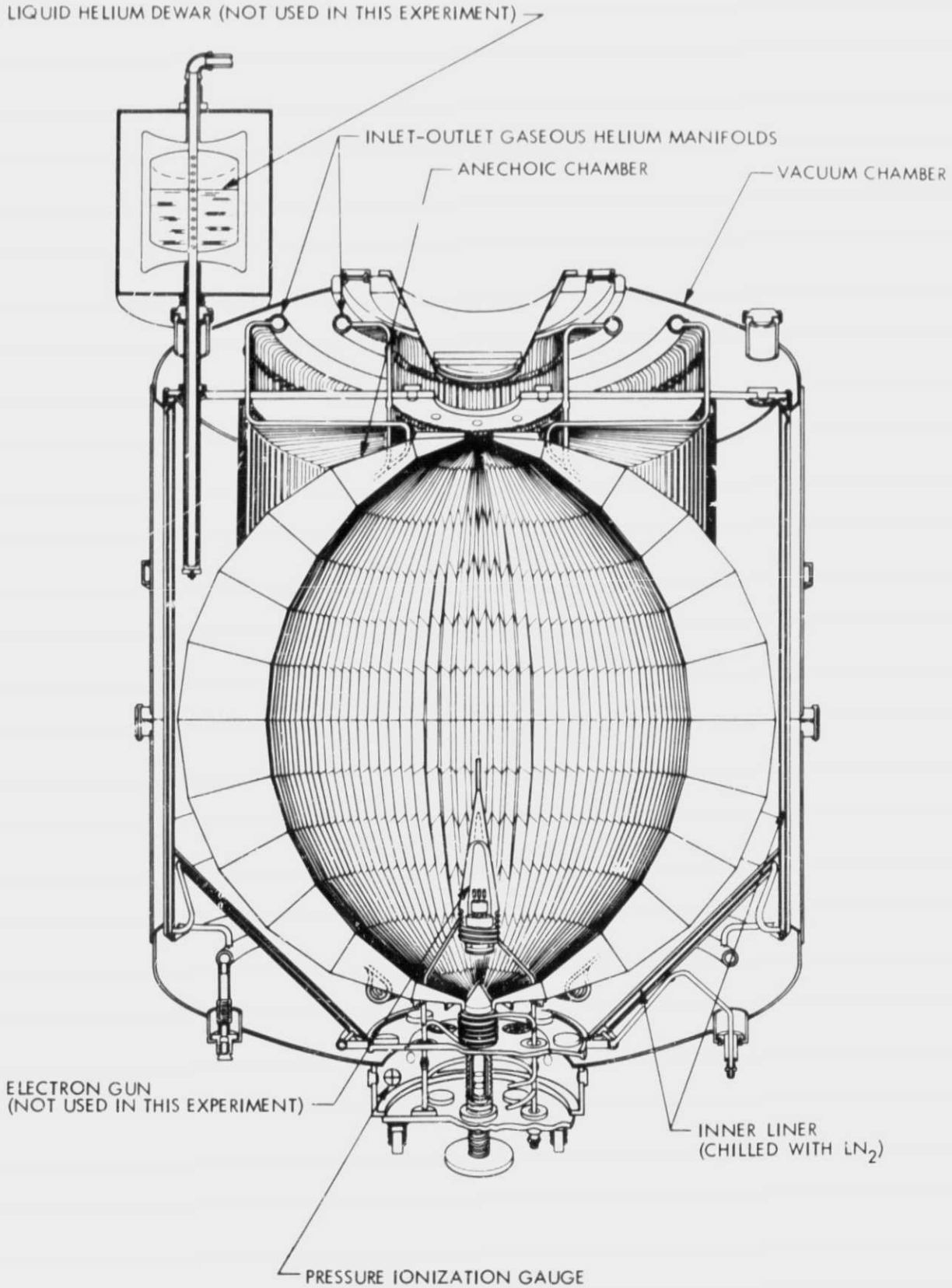

Fig. 1a. Molecular sink (Molsink) ultrahigh-vacuum chamber

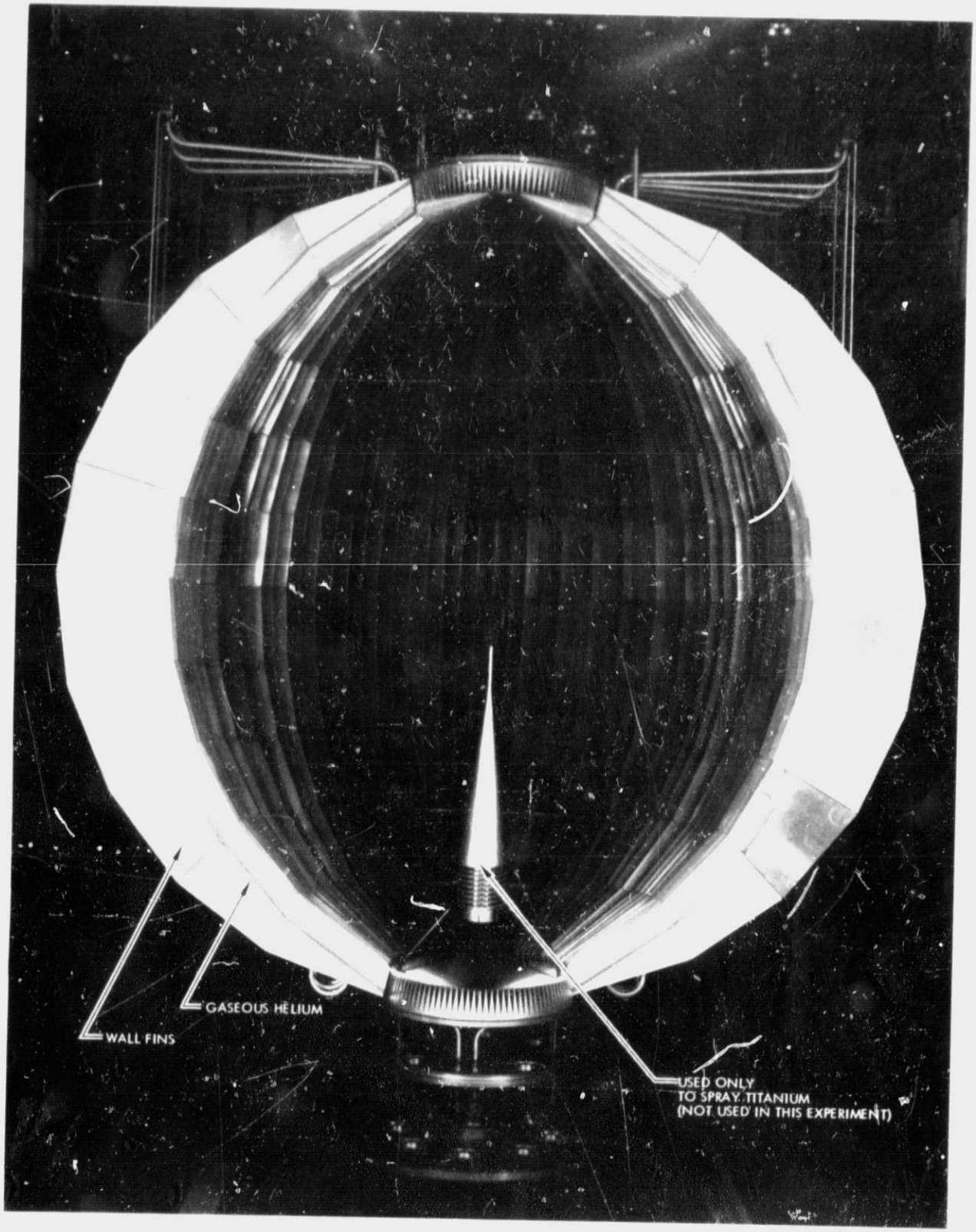

Fig. 1b. Molecular trap

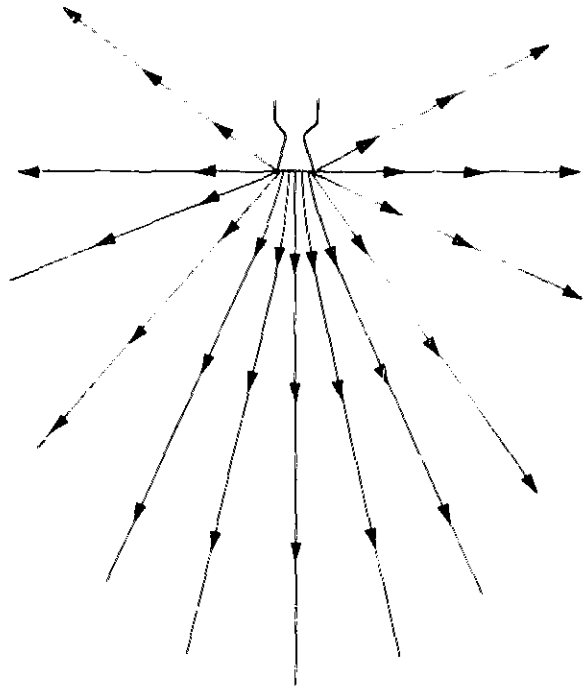

Fig. 2a. Rocket plume in space

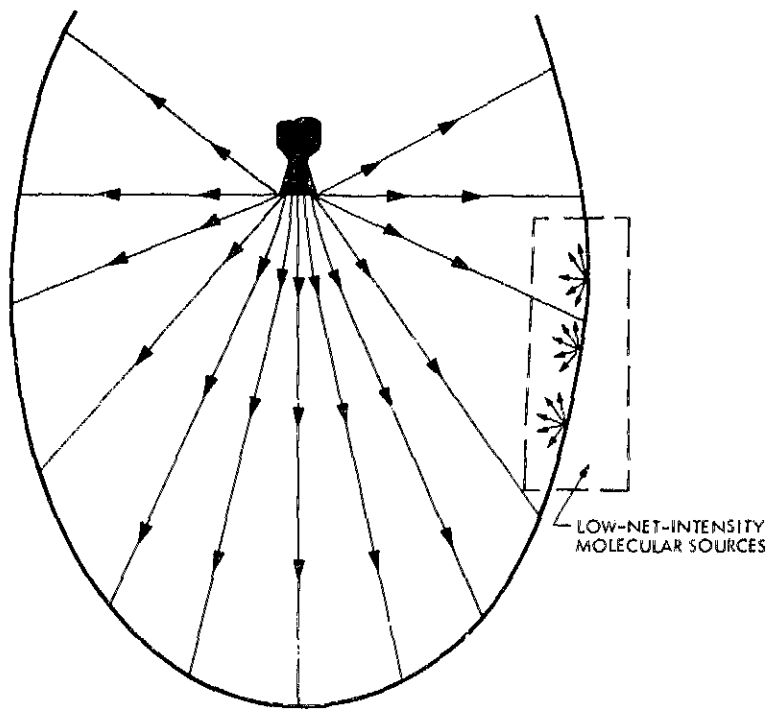

Fig. 2b. Rocket plume in Molsink chamber

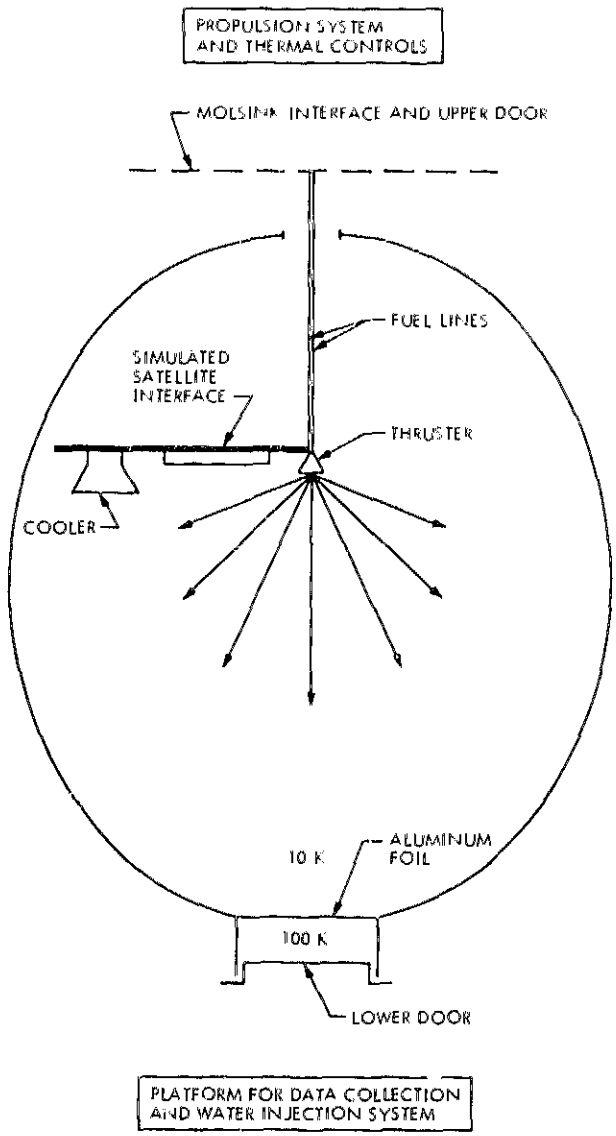

Fig. 3. General arrangement of the different systems in the Molsink (not to scale)

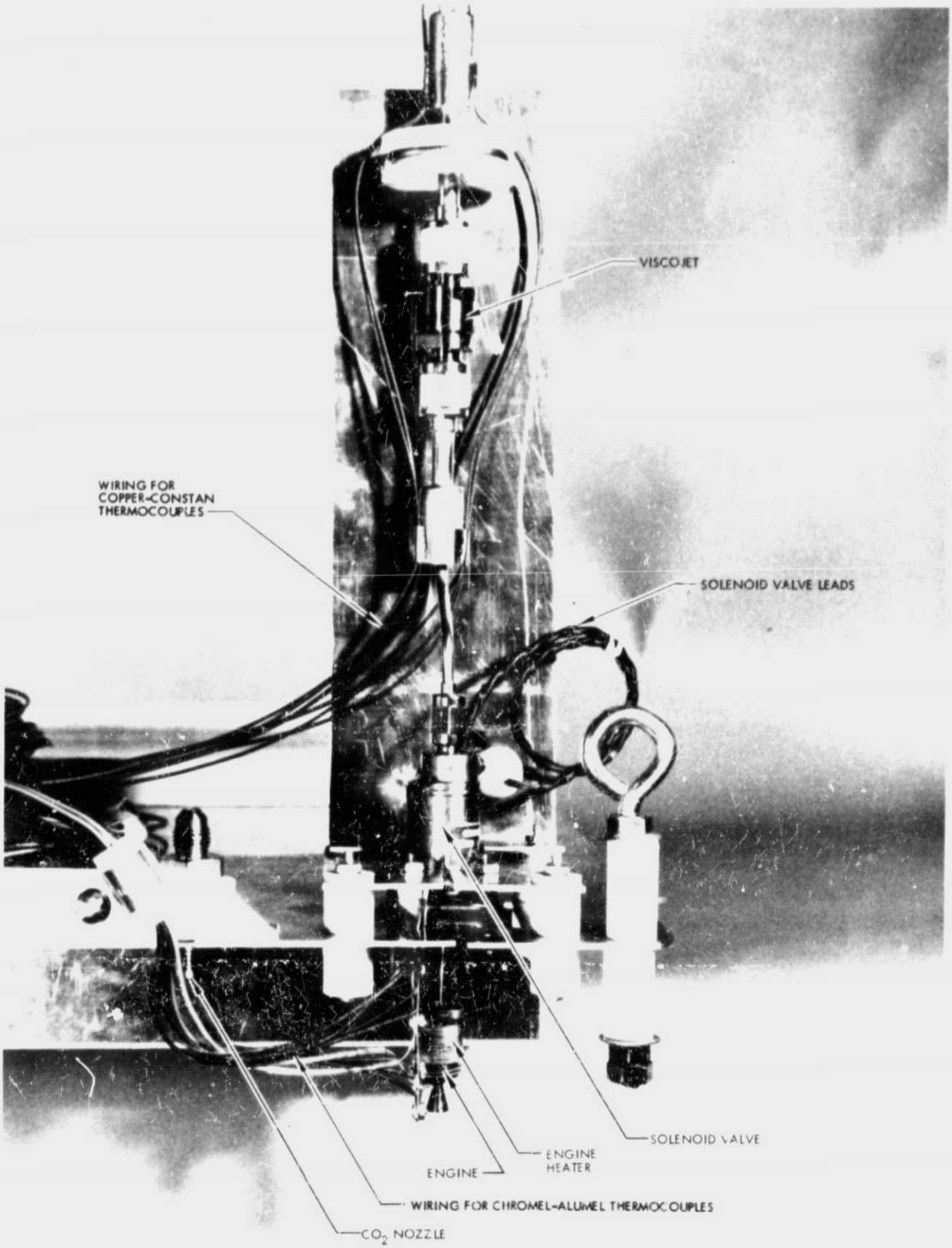

Fig. 4. Engine, valve, Viscojet, and thermocouples

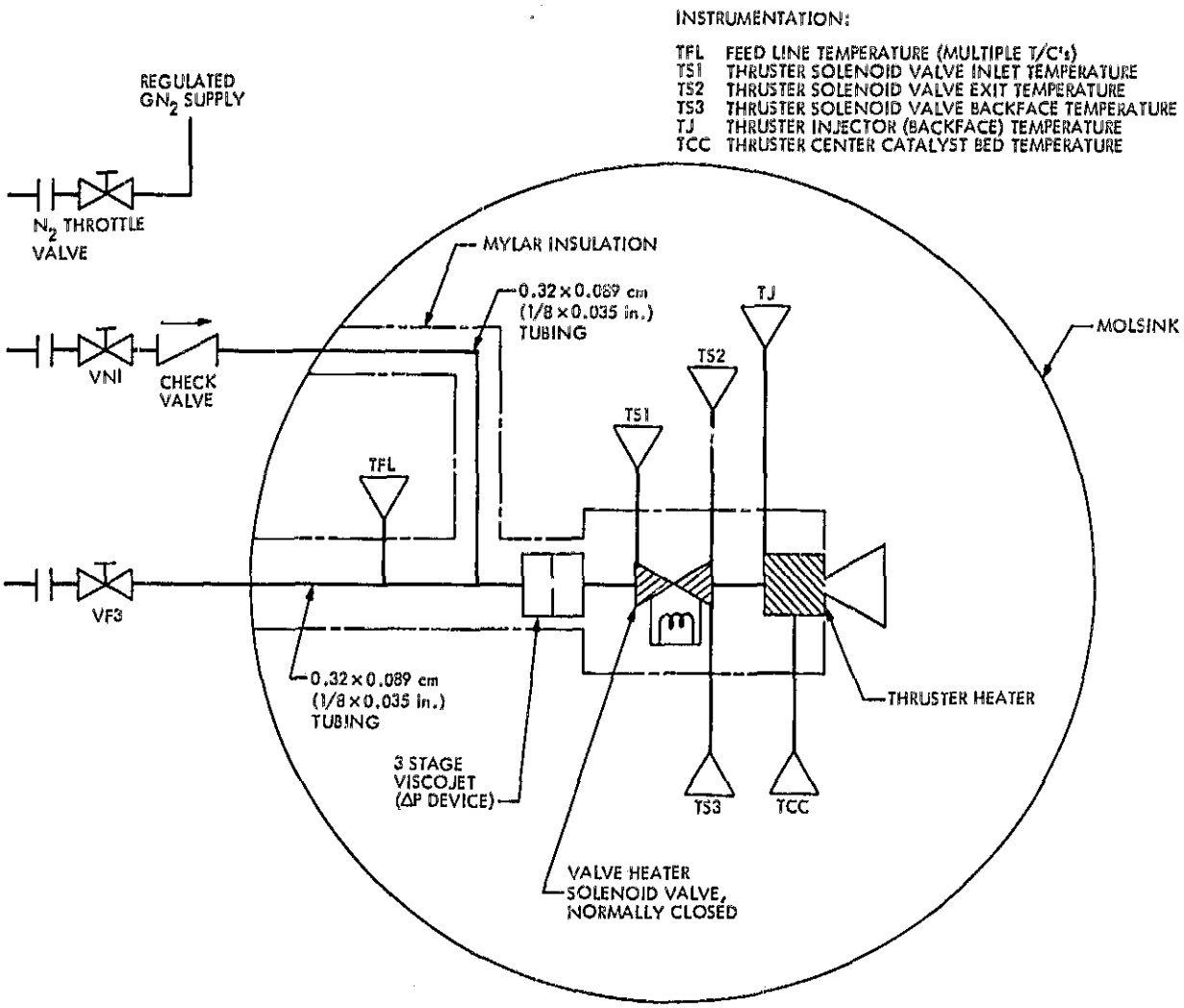

Fig. 5. Schematic diagram of propulsion subsystem inside the Molsink

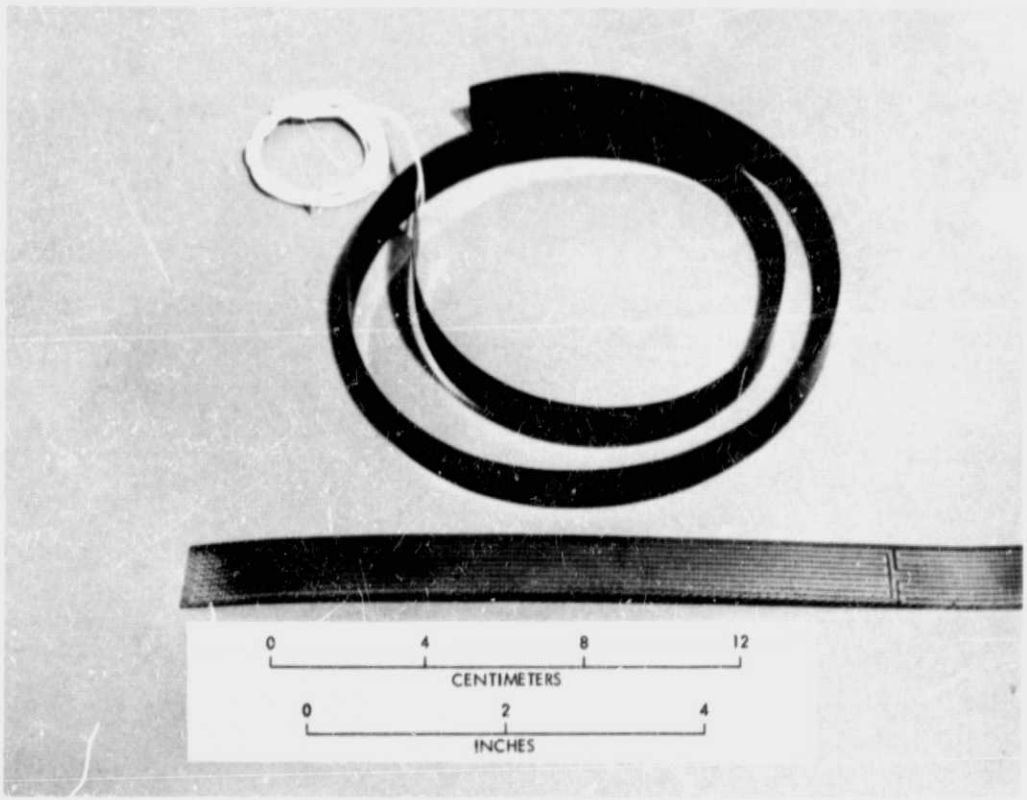

Fig. 6. Kapton Electrofilm heater

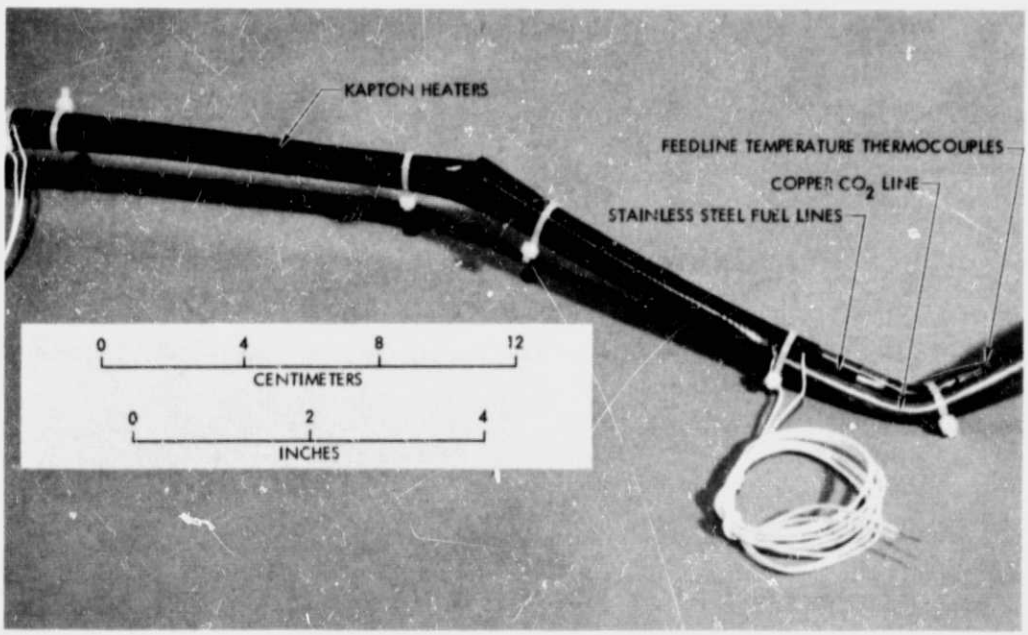

Fig. 7. Carbon dioxide and fuel lines thermal control system

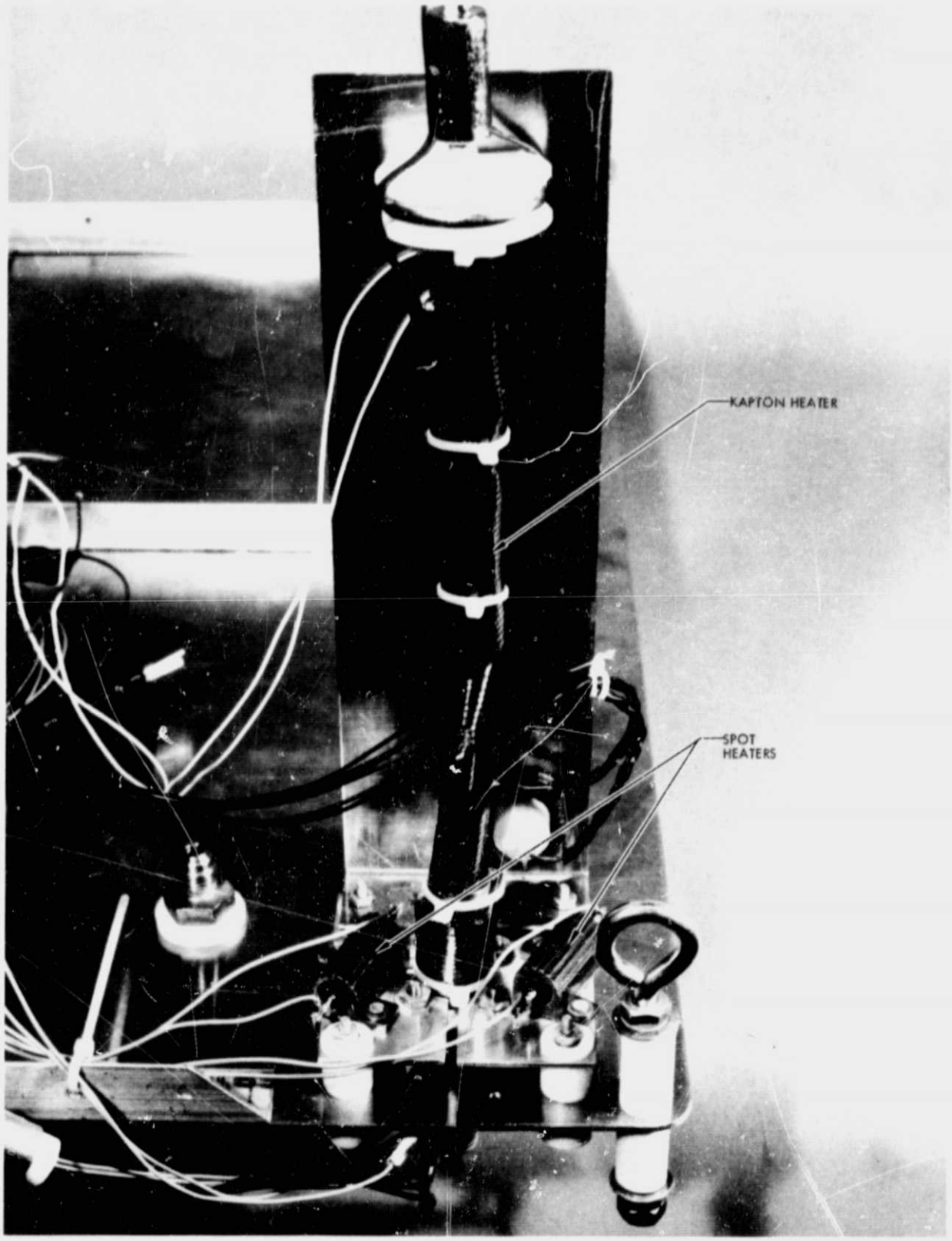

Fig. 8. Thermal control system on Viscojet, valve, and thruster

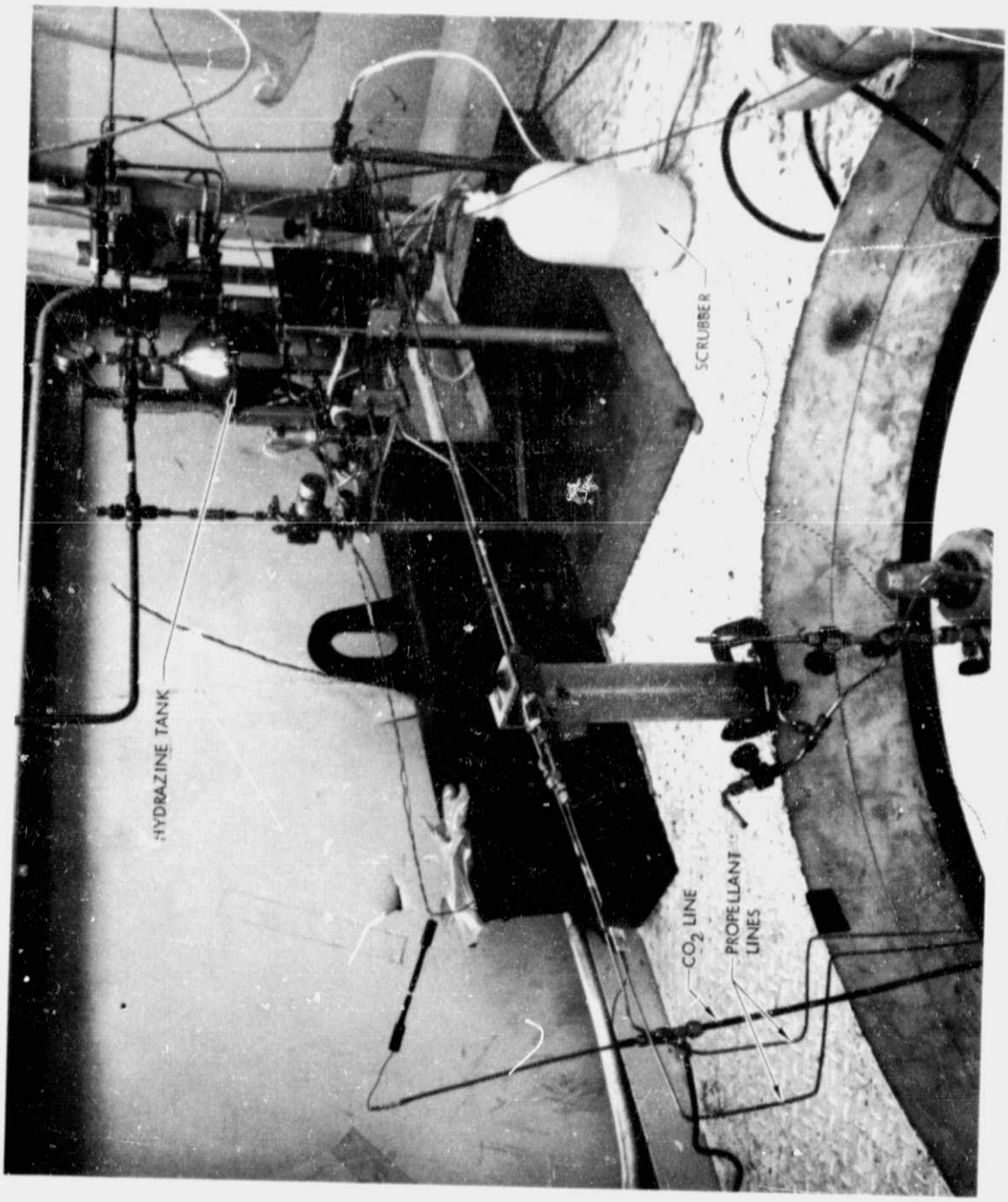

Fig. 9. Propellant feed module

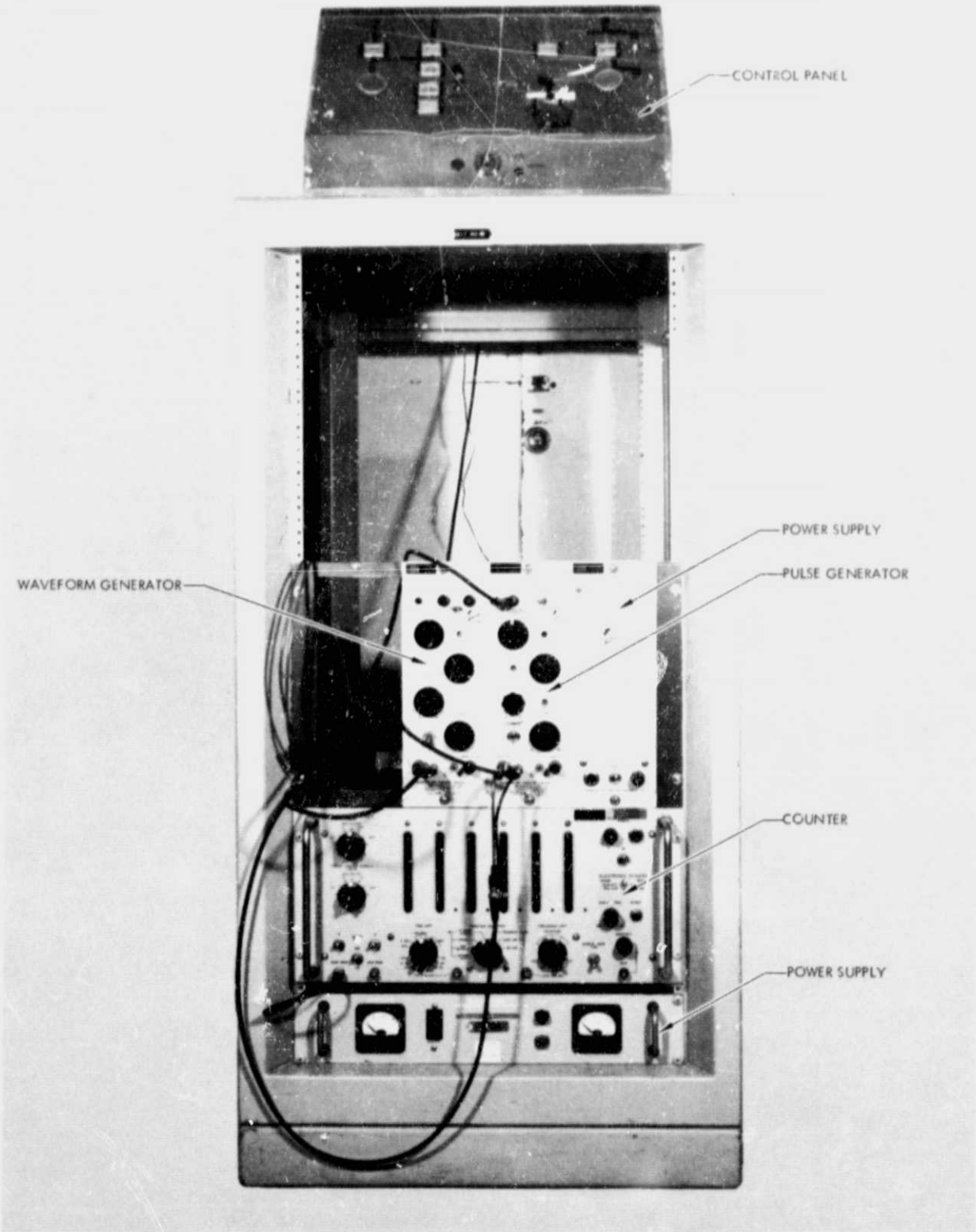

Fig. 10. Propulsion system control console

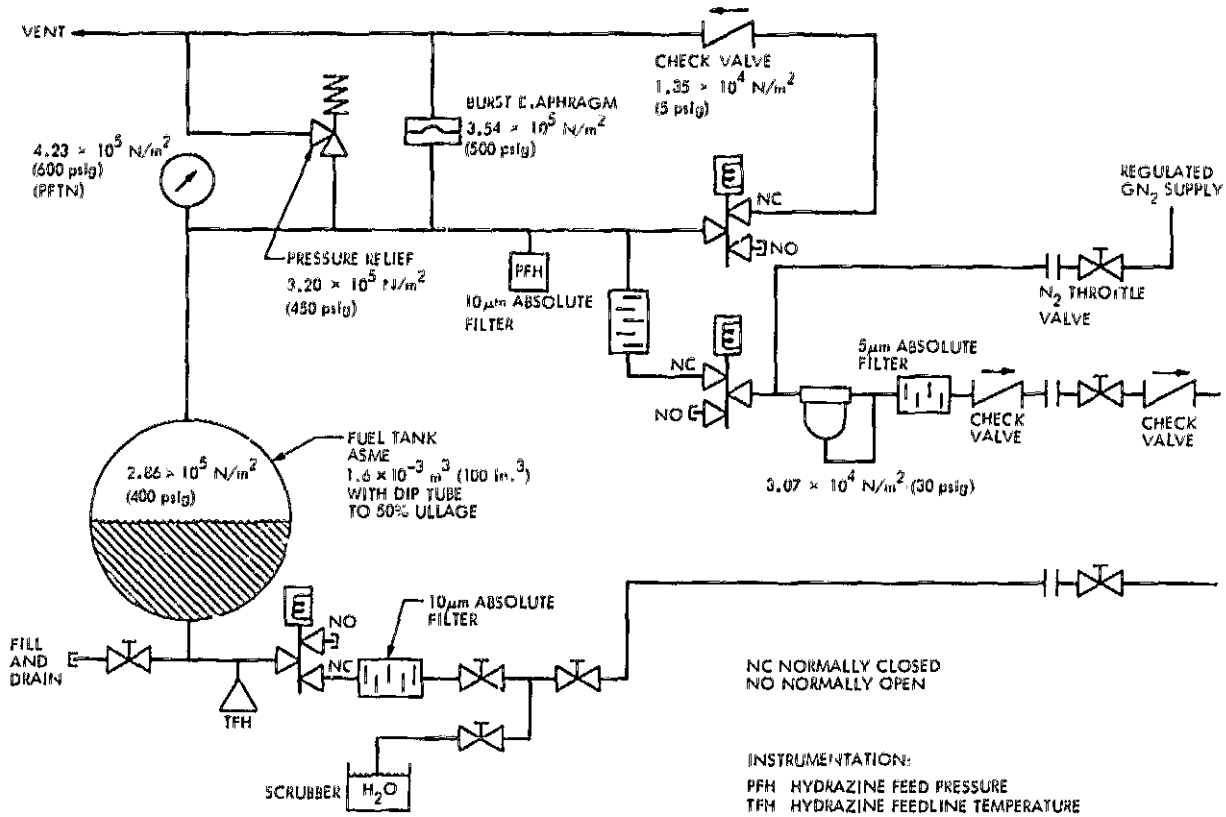

Fig. 11. Propulsion system schematic diagram

$$\Delta f = C_M \Delta M + C_T \Delta T$$

$C_M = \phi$(T, CUT ANGLES)

$C_T = \psi$(T, CUT ANGLES)

If $C_T \approx 0$, $\Delta M = \dfrac{\Delta f}{F_C^2} \times 4.35 \times 10^{-7}$

ΔM (gm/cm^2)

Δf (Hz)

F_C (MHz)

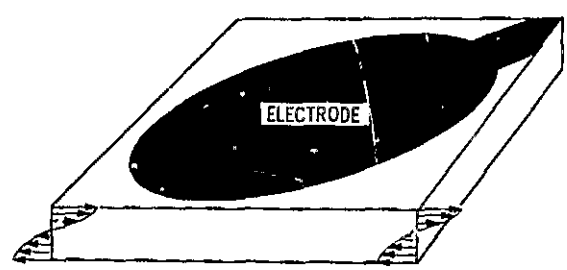

Fig. 12. Quartz crystal electrodes and demonstration of the thickness vibration mode

$$\Delta f_1 = C_{M_1} \Delta M_1 + C_{T_1} \Delta T_1$$

$$\Delta f_2 = C_{M_2} \Delta M_2 + C_{T_2} \Delta T_2$$

$$\left.\begin{aligned} C_{M_1} &= C_{M_2} \\ C_{T_1} &= C_{T_2} \end{aligned}\right\} \text{ if } T_1 = T_2$$

$$\Delta F = \Delta f_1 - \Delta f_2 = C_{M_1} \Delta M_1$$

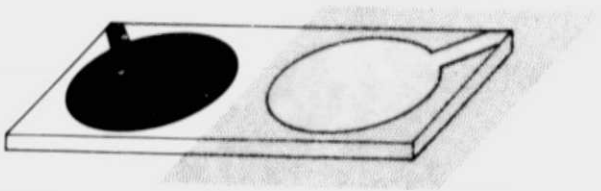

Fig. 13. Doublet QCM

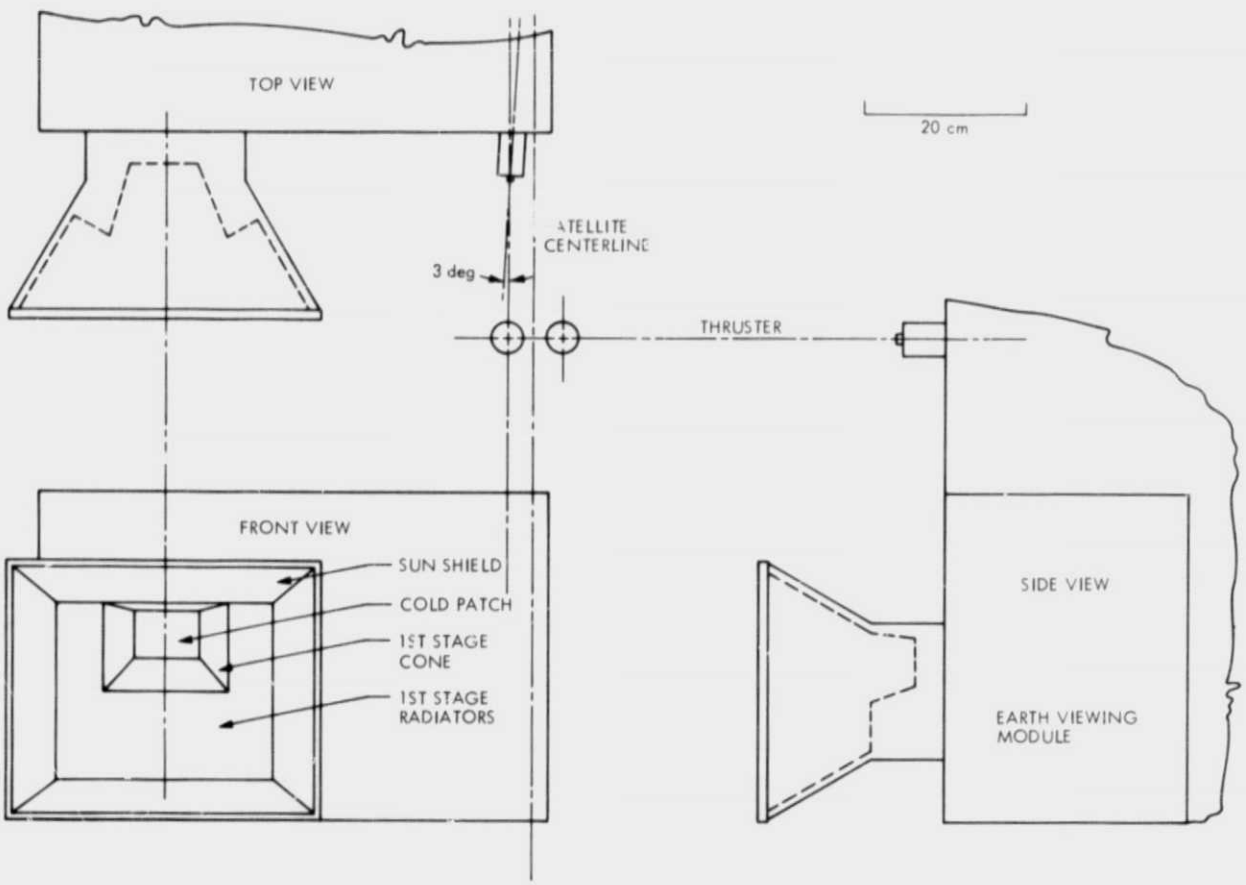

Fig. 14. Three views of the radiant cooler and its relative position with respect to the thruster and satellite

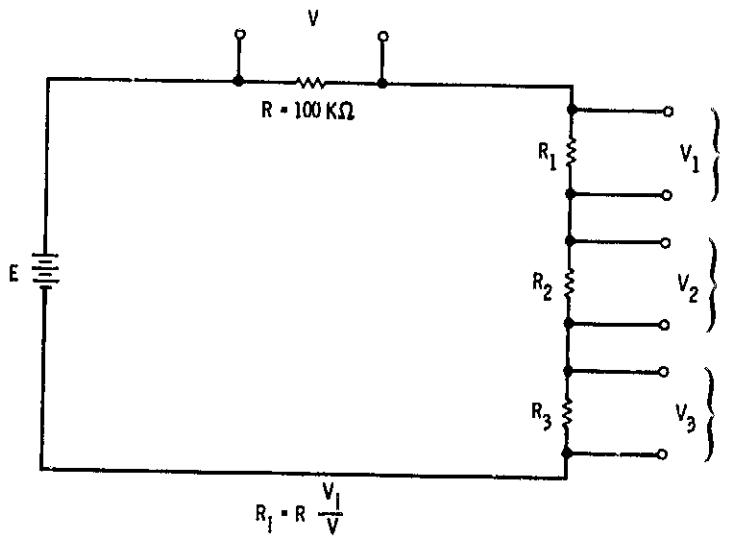

Fig. 15. Schematic diagram for the platinum sensors

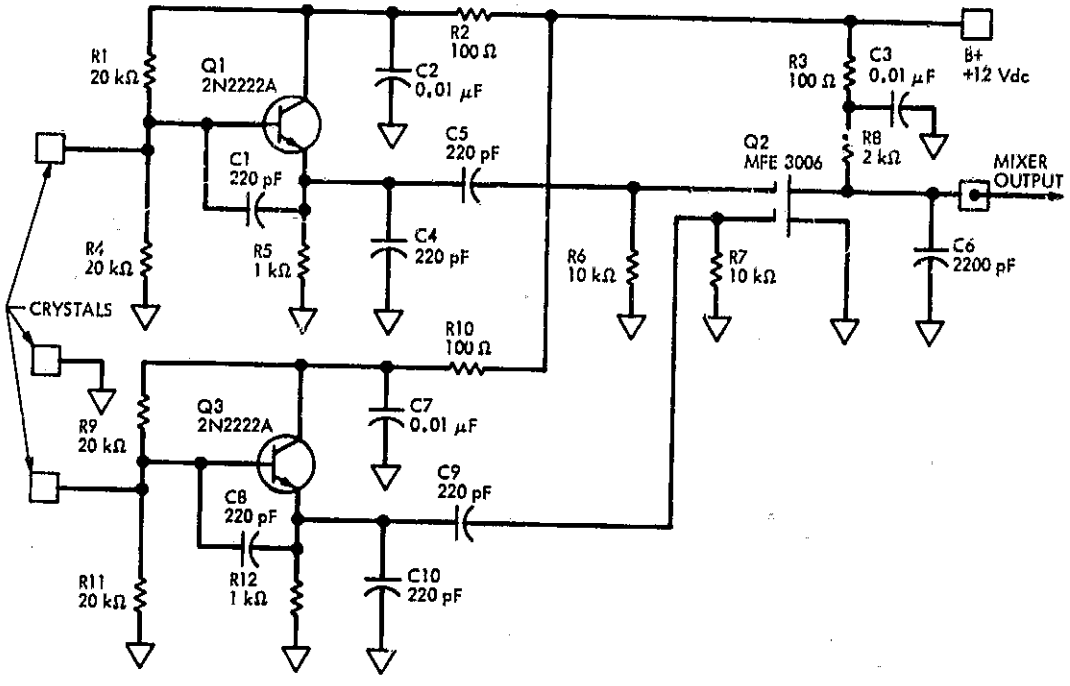

Fig. 16. Hybrid circuit for doublet QCM

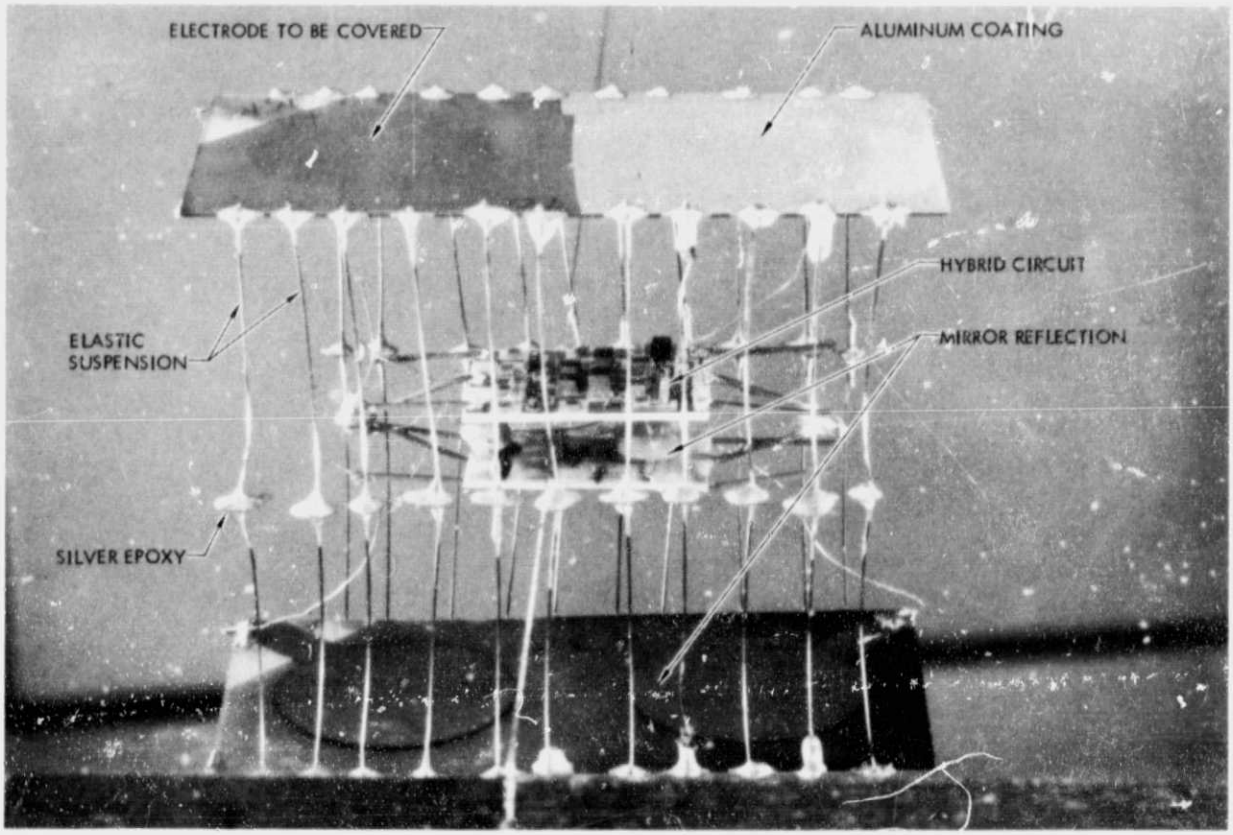

Fig. 17a. Photograph of an unfinished QCM doublet and hybrid circuit mounted on the sun shield surface

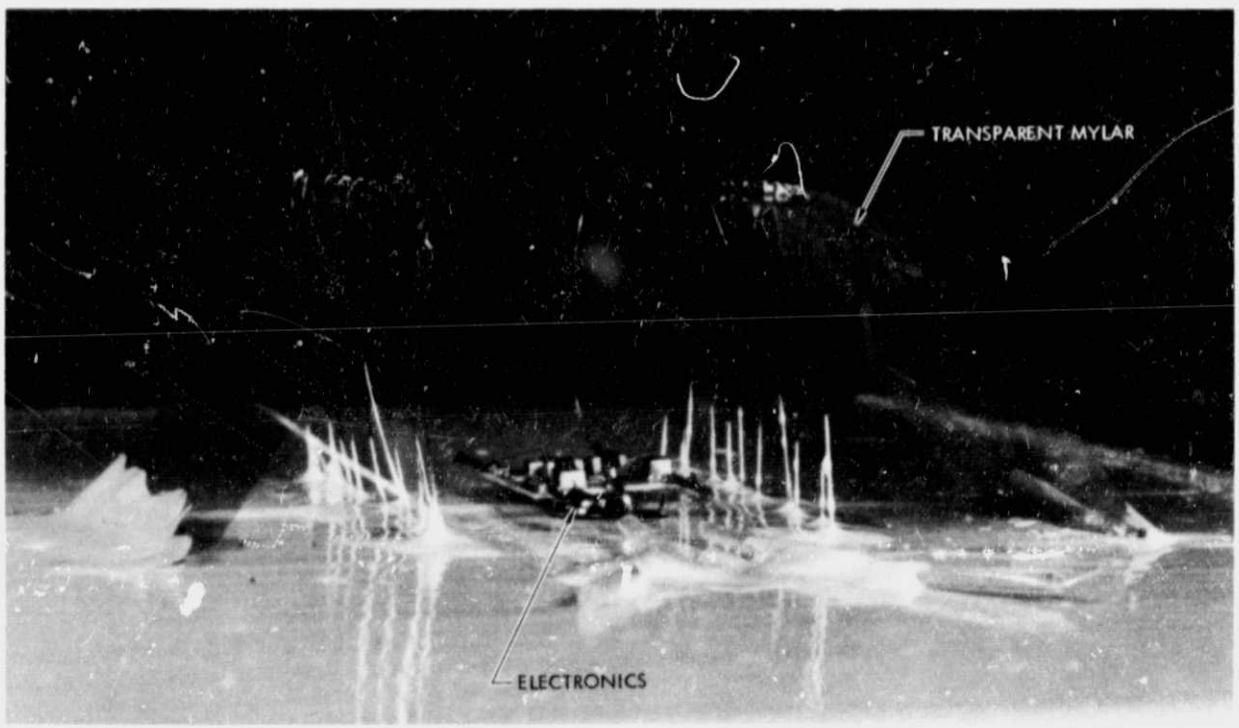

Fig. 17b. Photograph of a complete QCM mounted on the first-stage radiator surface

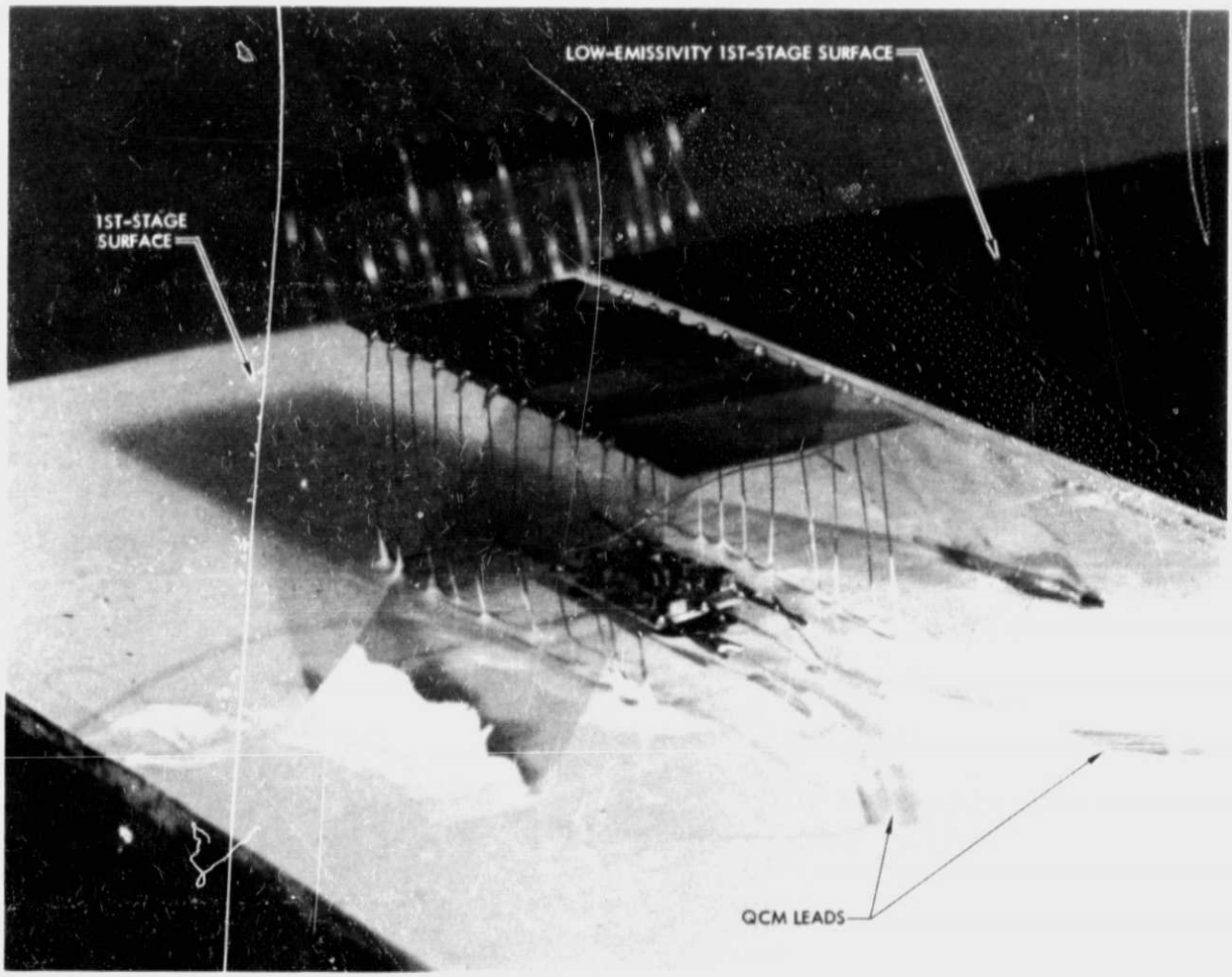

Fig. 17c. Another view of a temperature-compensated, low-optical-obstruction QCM

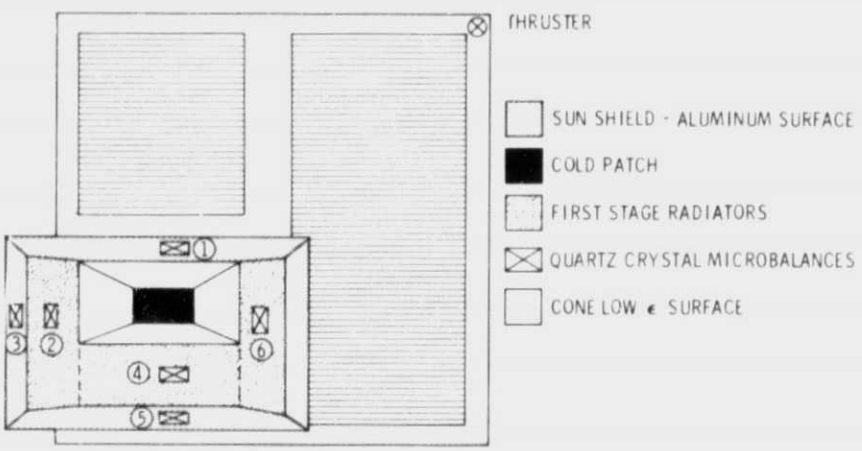

Fig. 18. General overview of the tested assembly

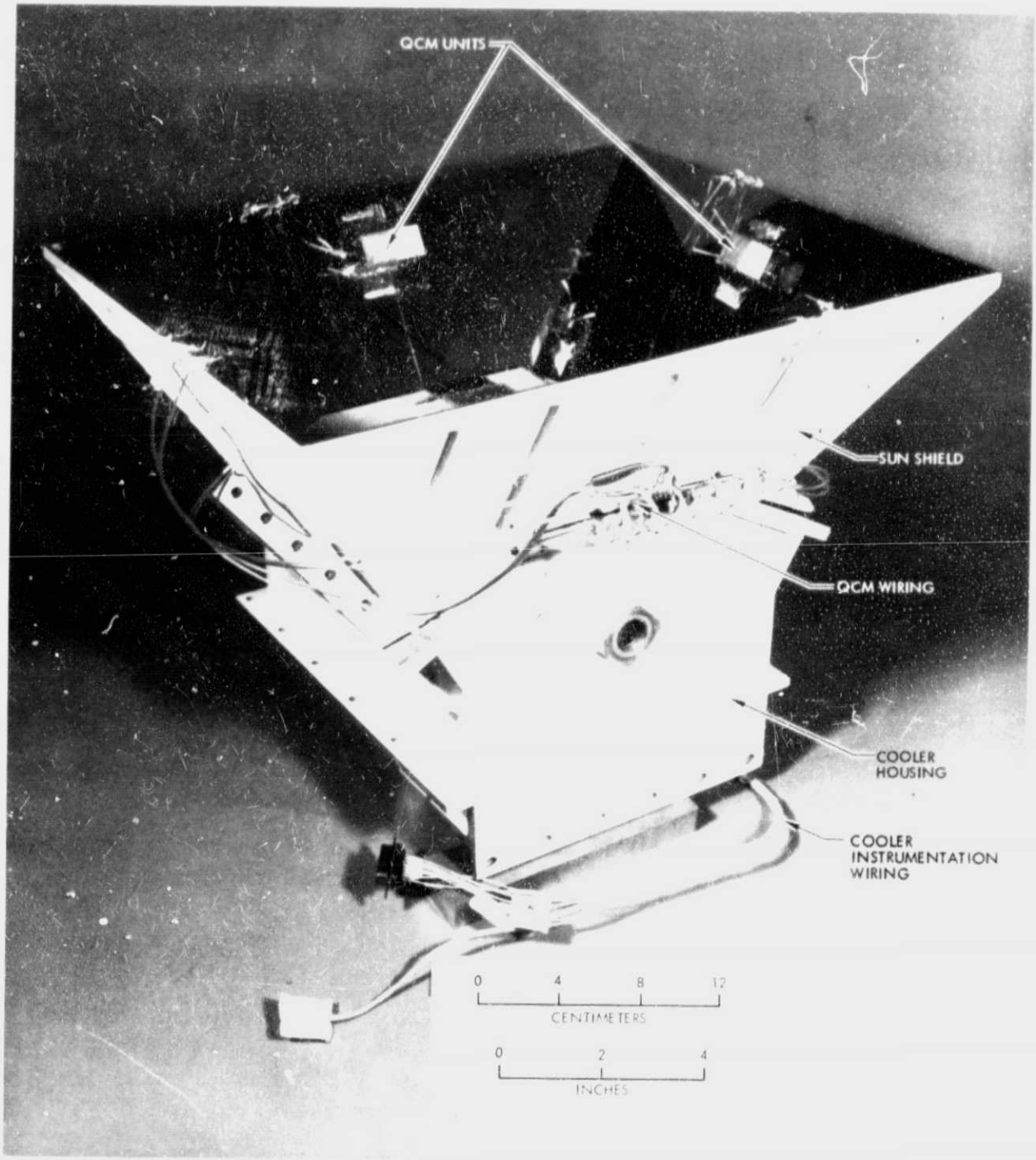

Fig. 19a. A view of the radiant cooler instrumented with QCMs

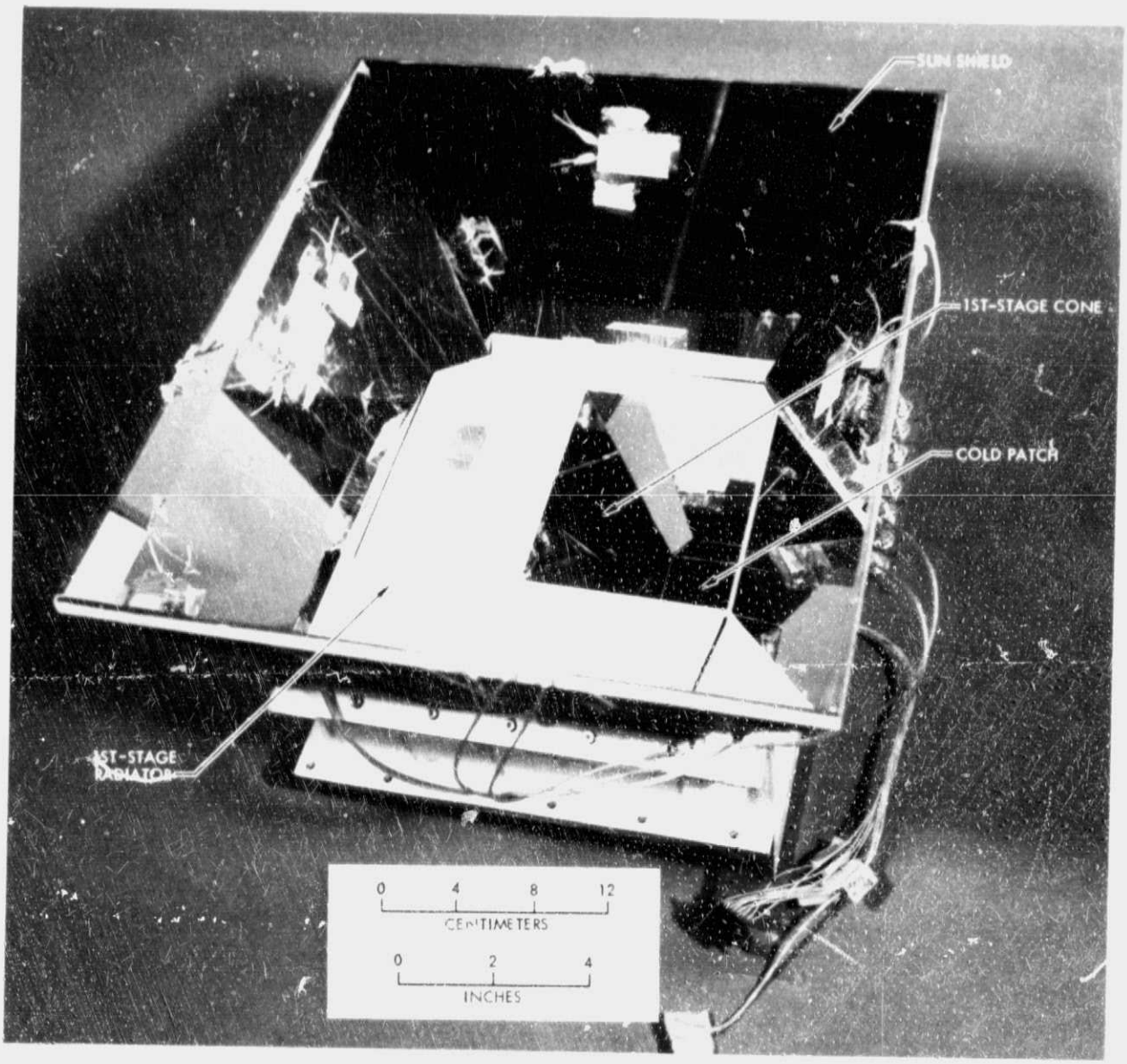

Fig. 19b. An oblique view of the radiant cooler and the QCM positions

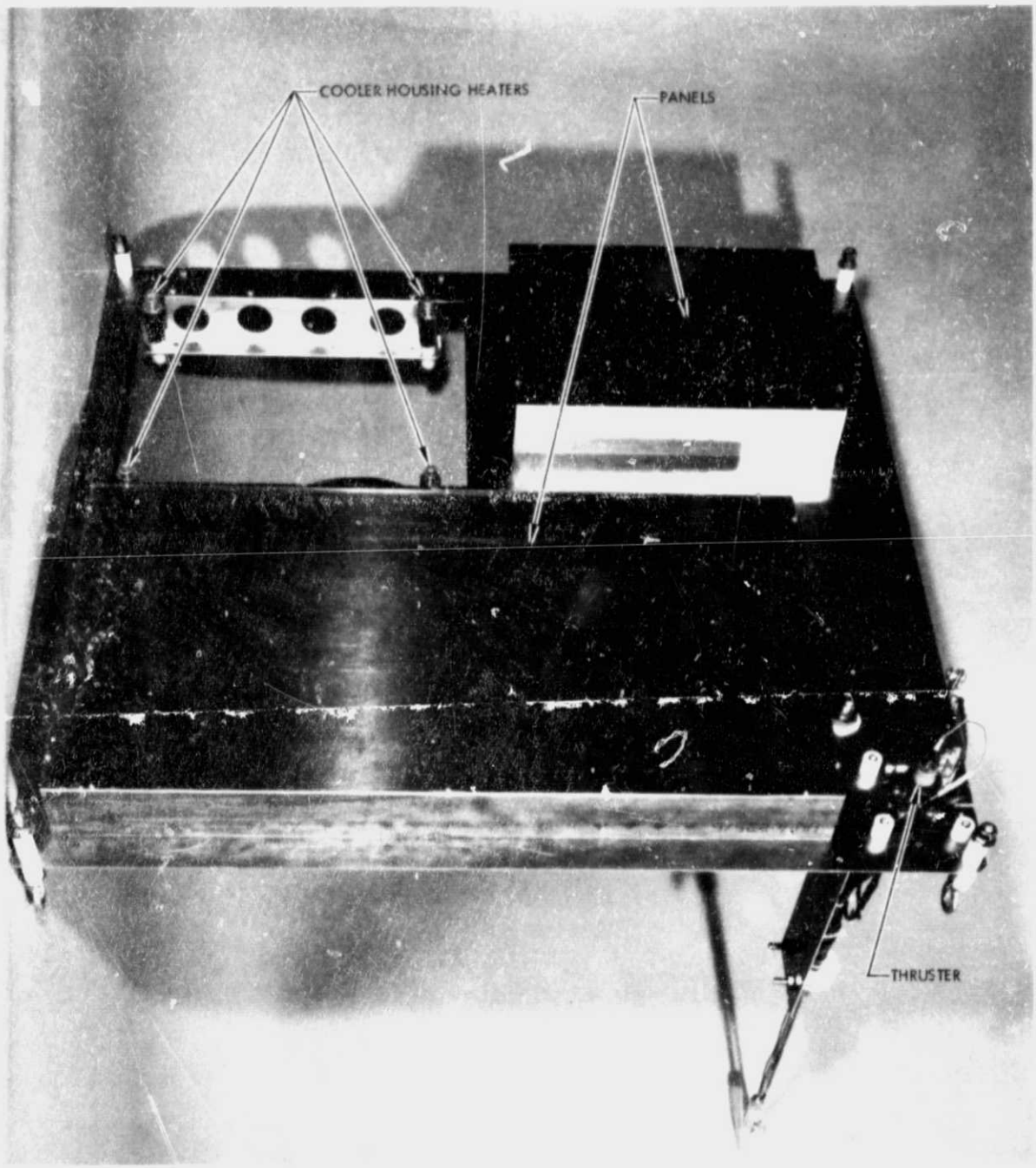

Fig. 20a. Mock-up of satellite segment to be assembled with thruster and cooler (front view)

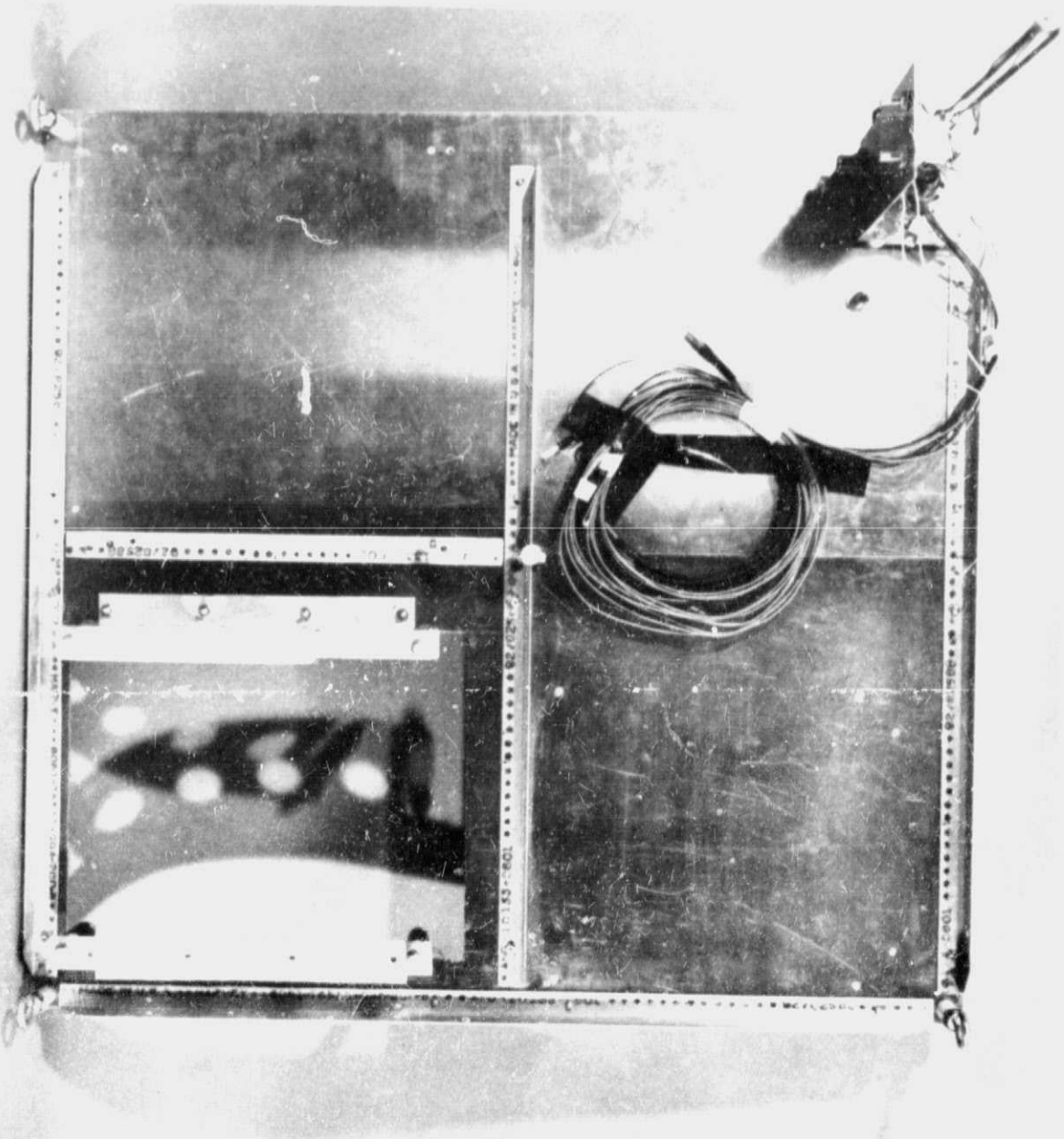

Fig. 20b. Mock-up of satellite segment to be assembled with thruster and cooler (rear view)

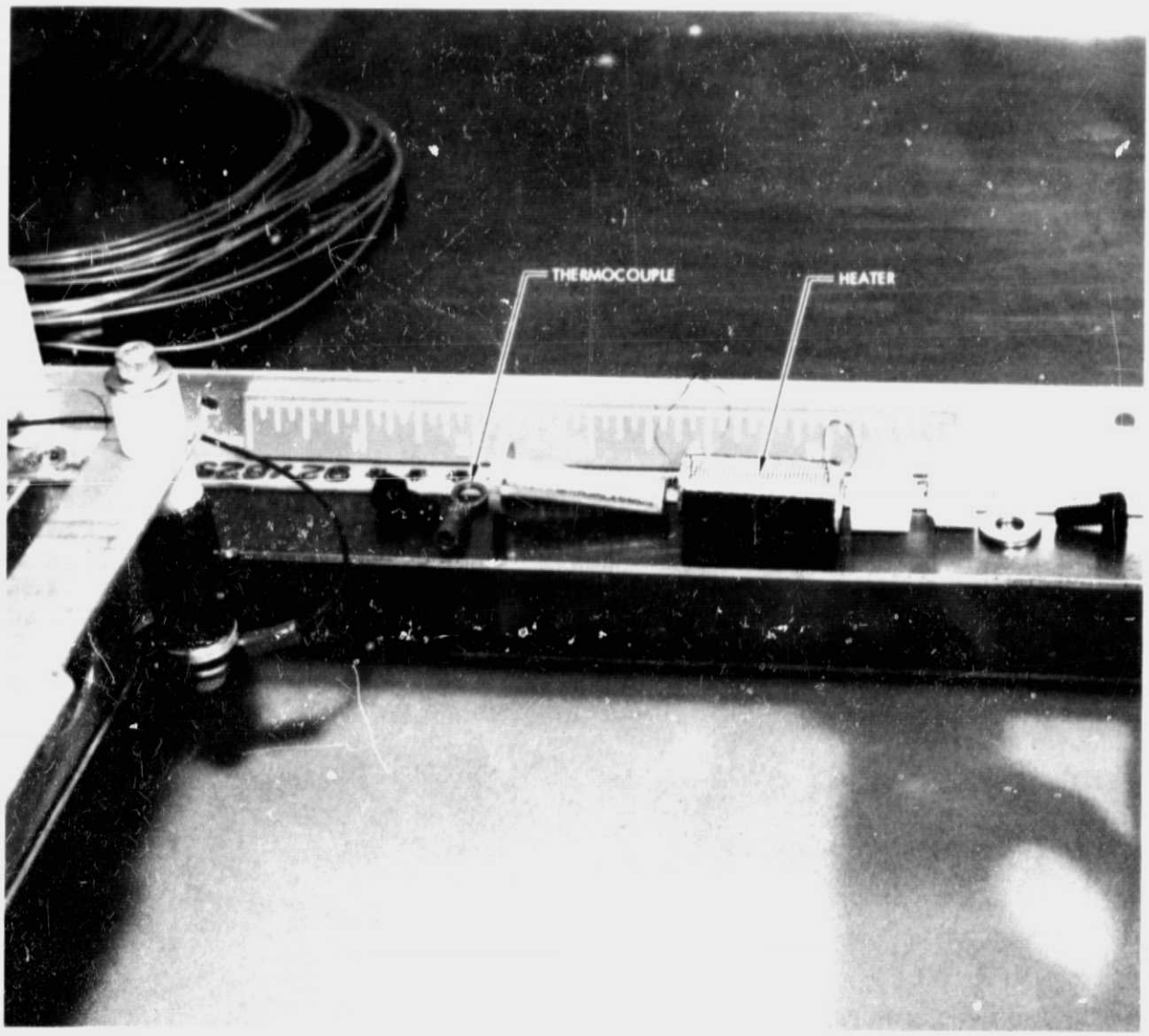

Fig. 20c. Details of the ceramic heater and thermocouple installation for thermal control of the cooler housing

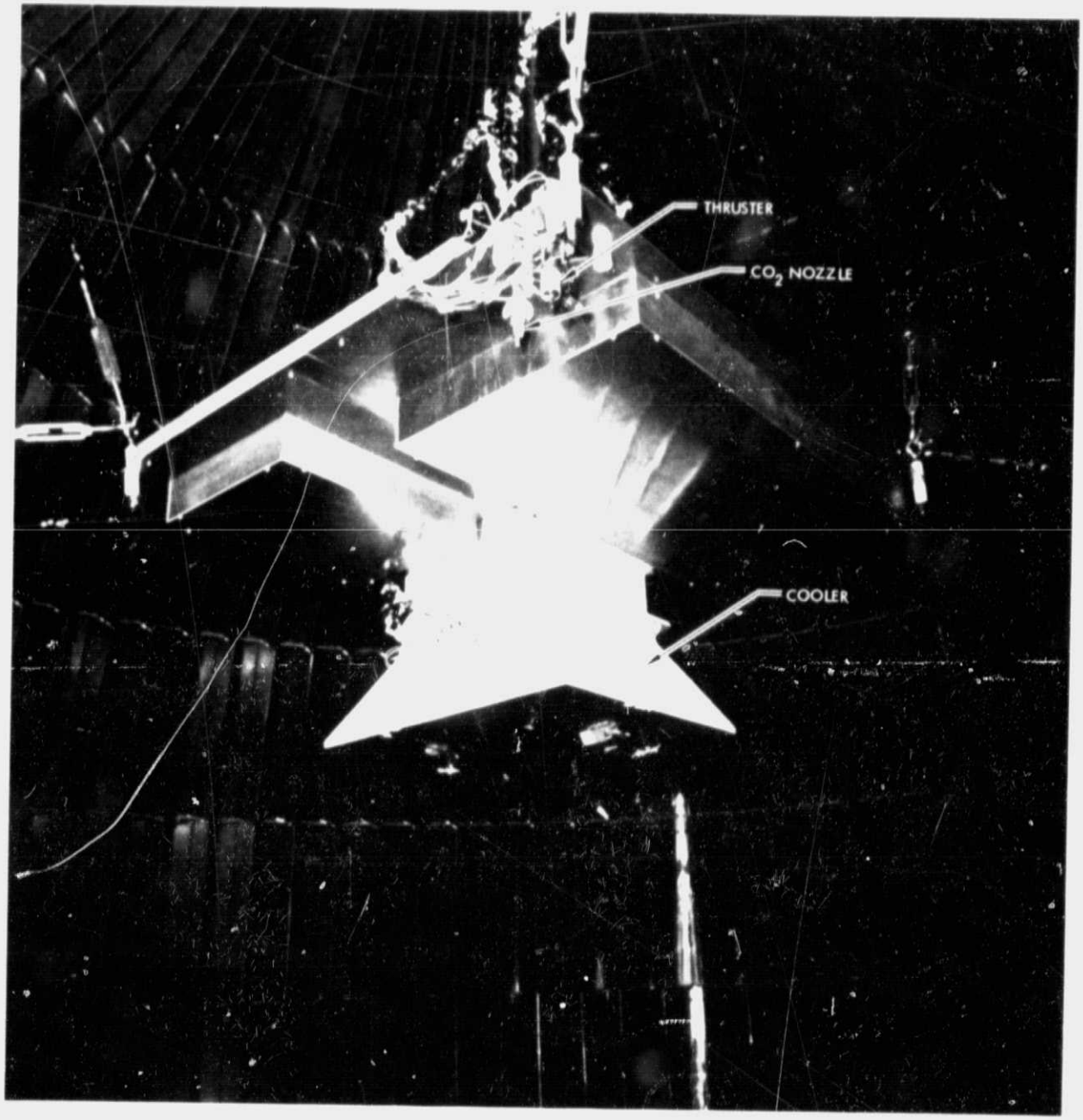

Fig. 21a. Assembled package (side view)

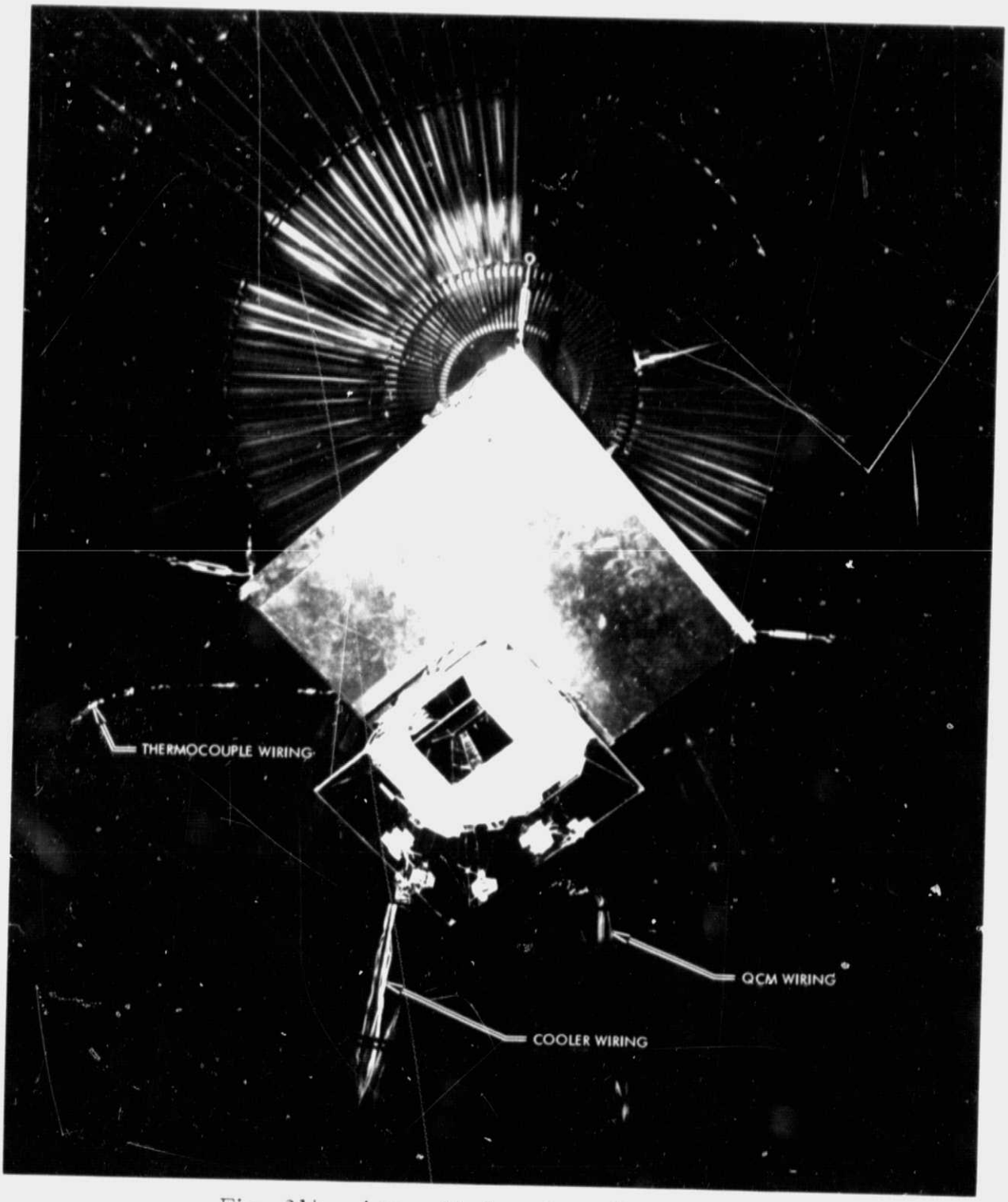

Fig. 21b. Assembled package (front view)

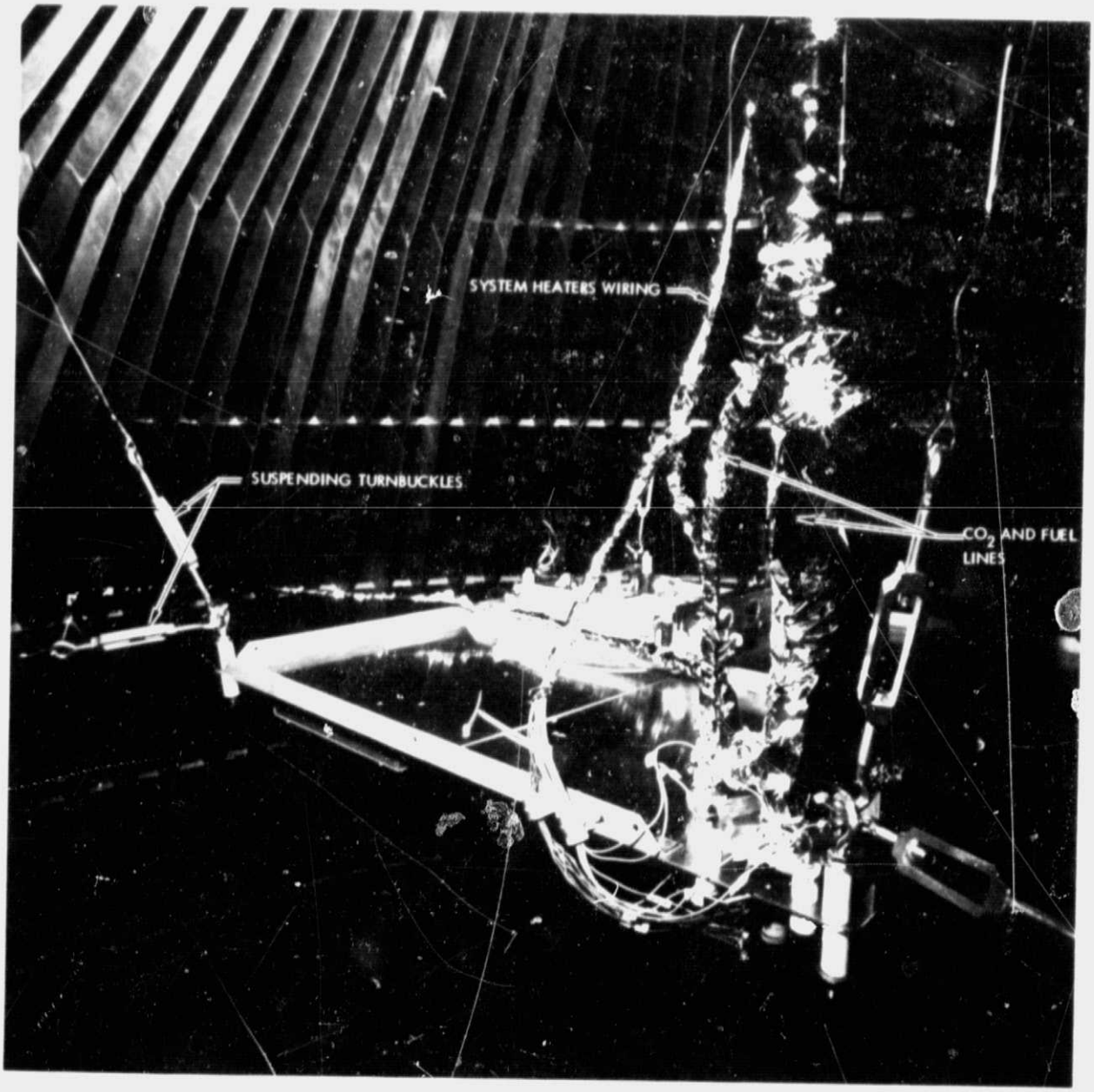

Fig. 22a. Assembled package (rear view)

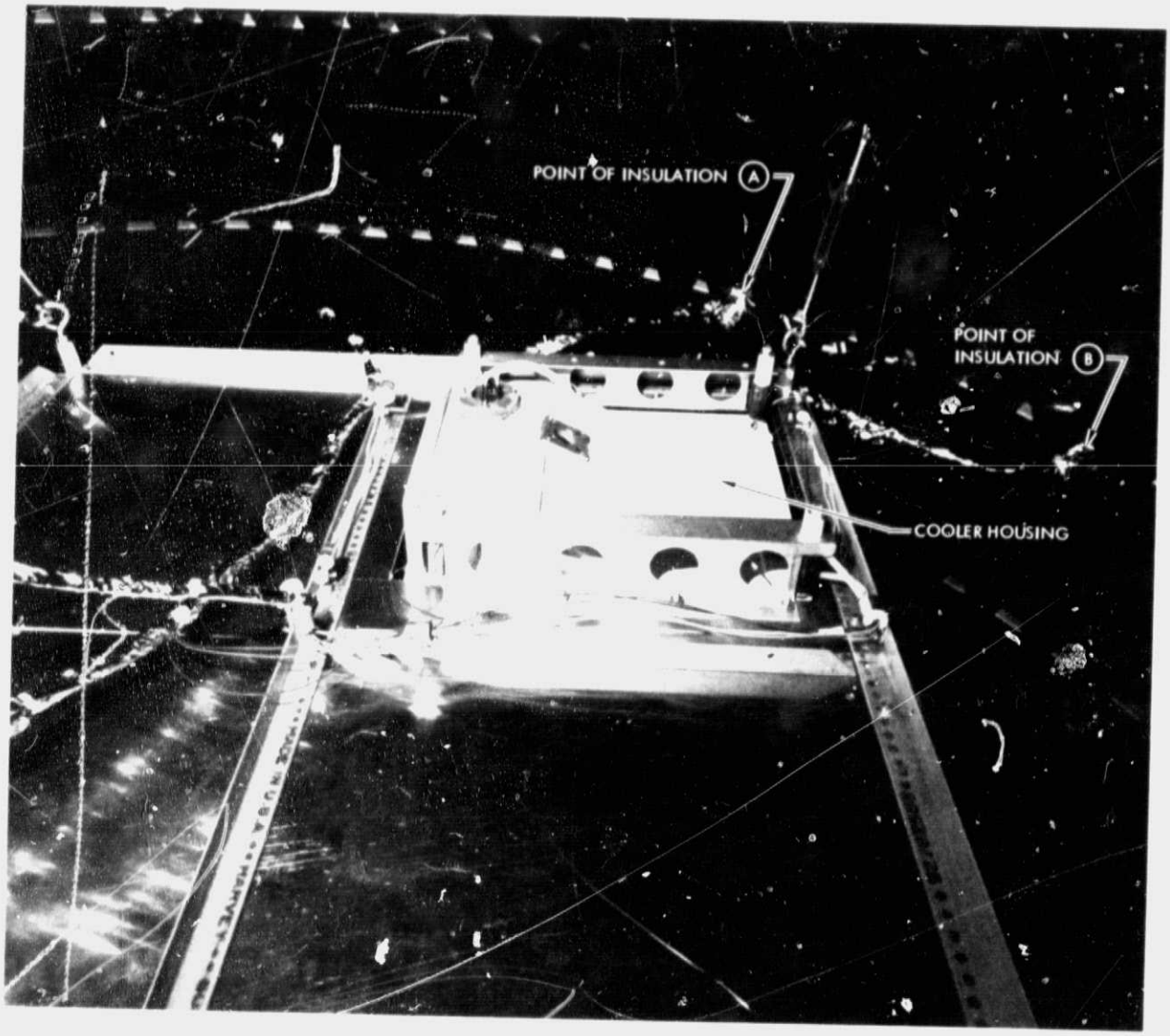

Fig. 22b. Radiant cooler installation (rear view)

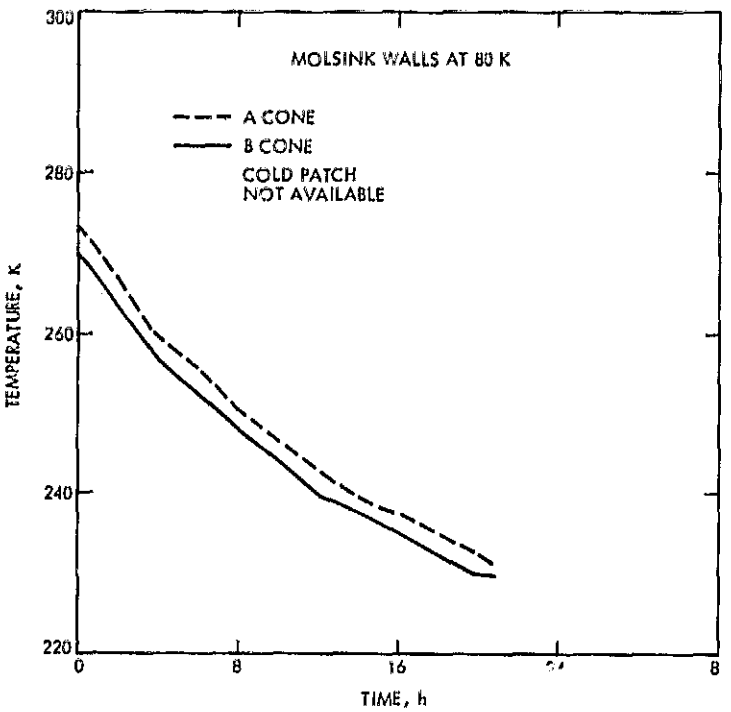

Fig. 23. Radiant cooler temperature variations, August 12, 1972

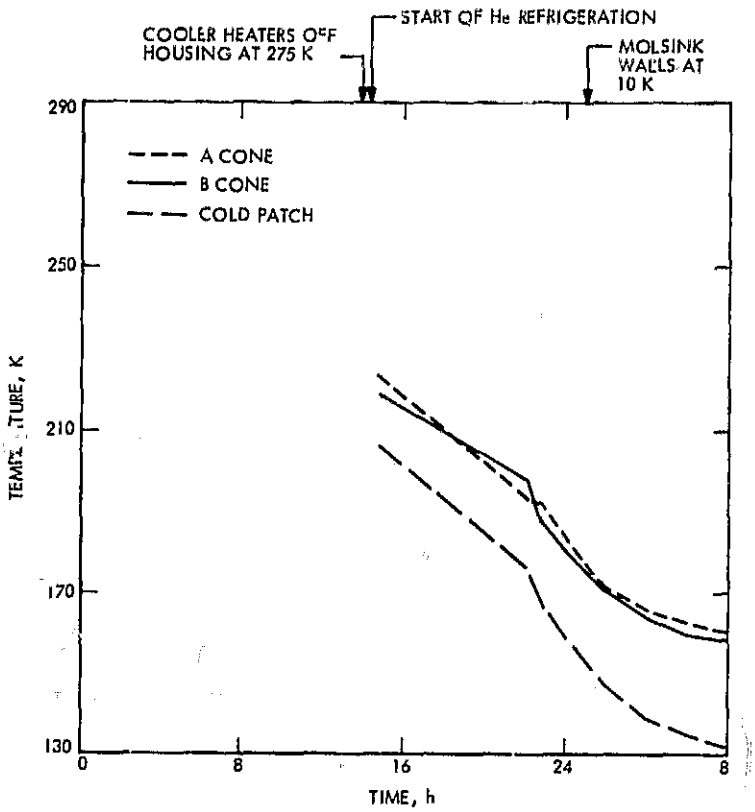

Fig. 24. Radiant cooler temperature variations, August 13, 1972

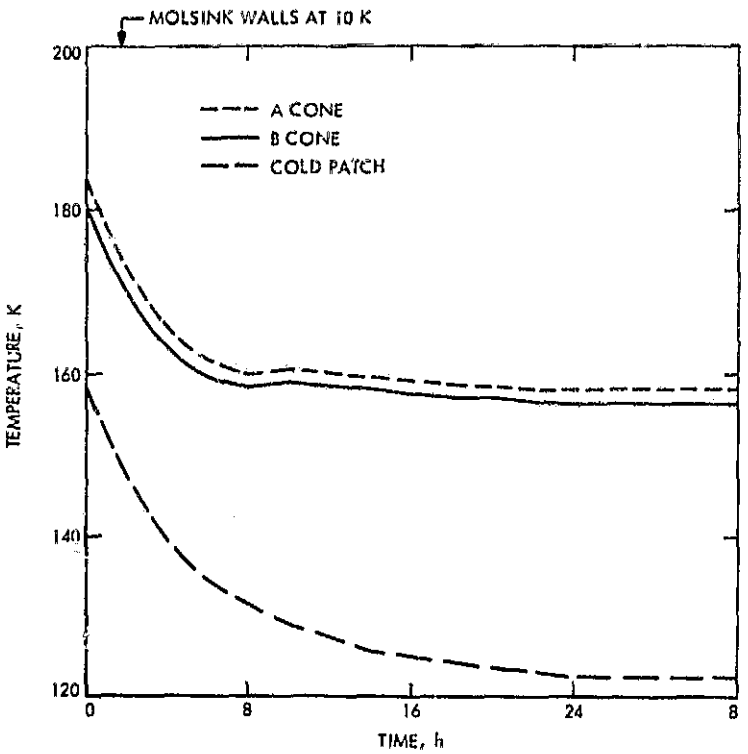

Fig. 25. Radiant cooler temperature variations, August 14, 1972

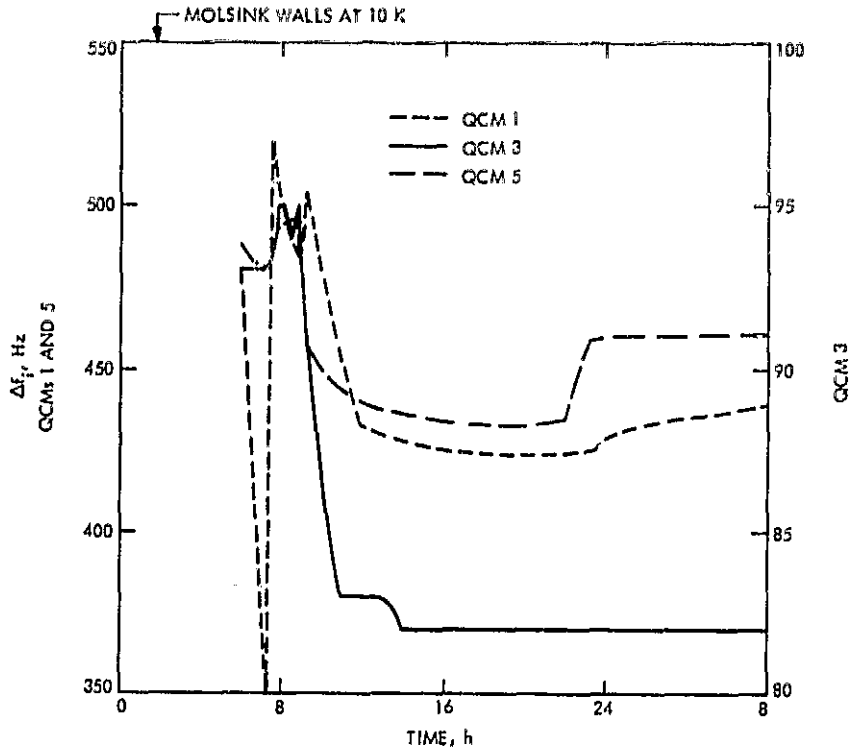

Fig. 26a. Frequency variation of sun shield QCMs, August 14, 1972

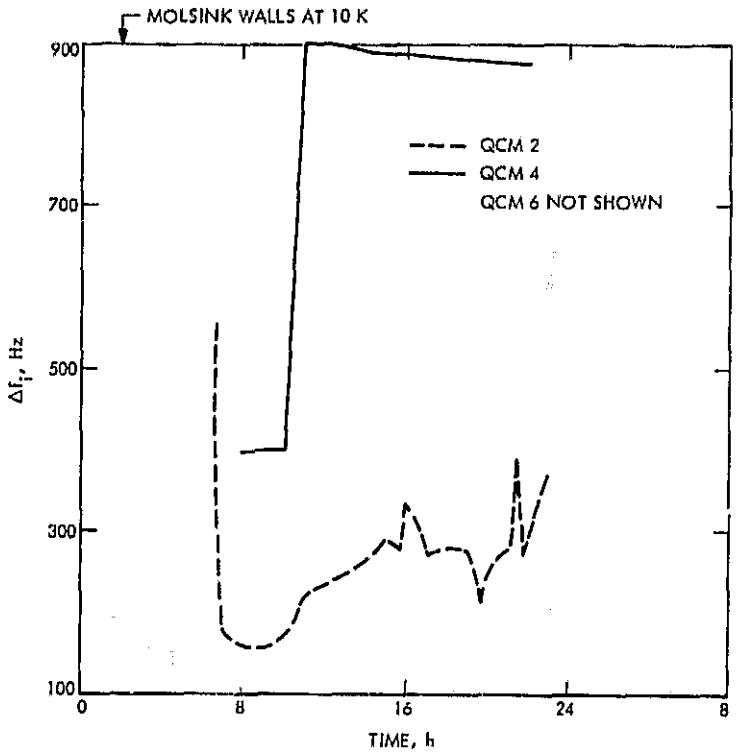

Fig. 26b. Frequency variation of radiant cooler QCMs, August 14, 1972

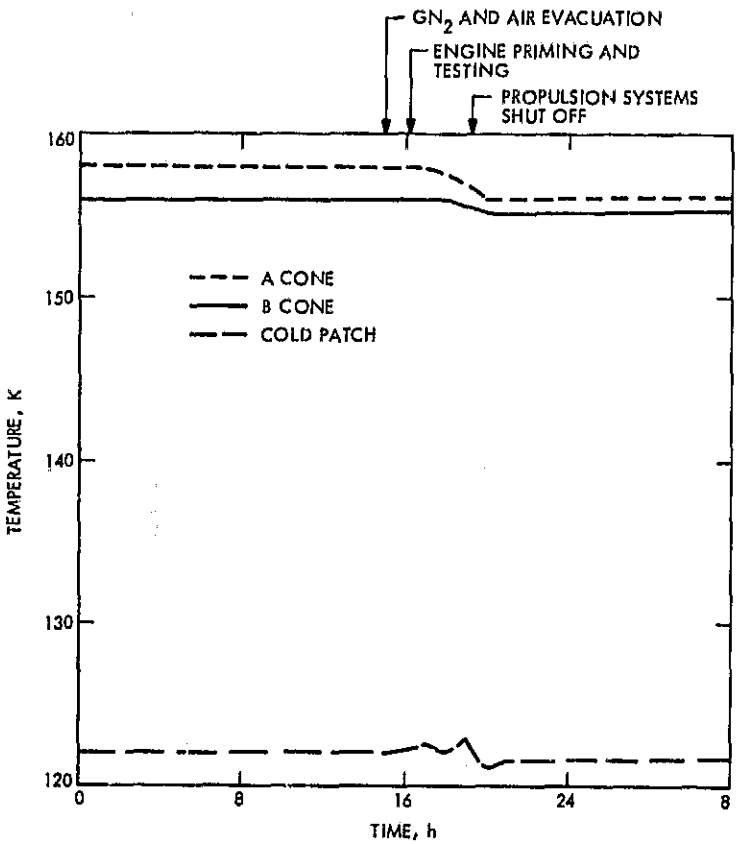

Fig. 27. Radiant cooler temperature variations, August 15, 1972

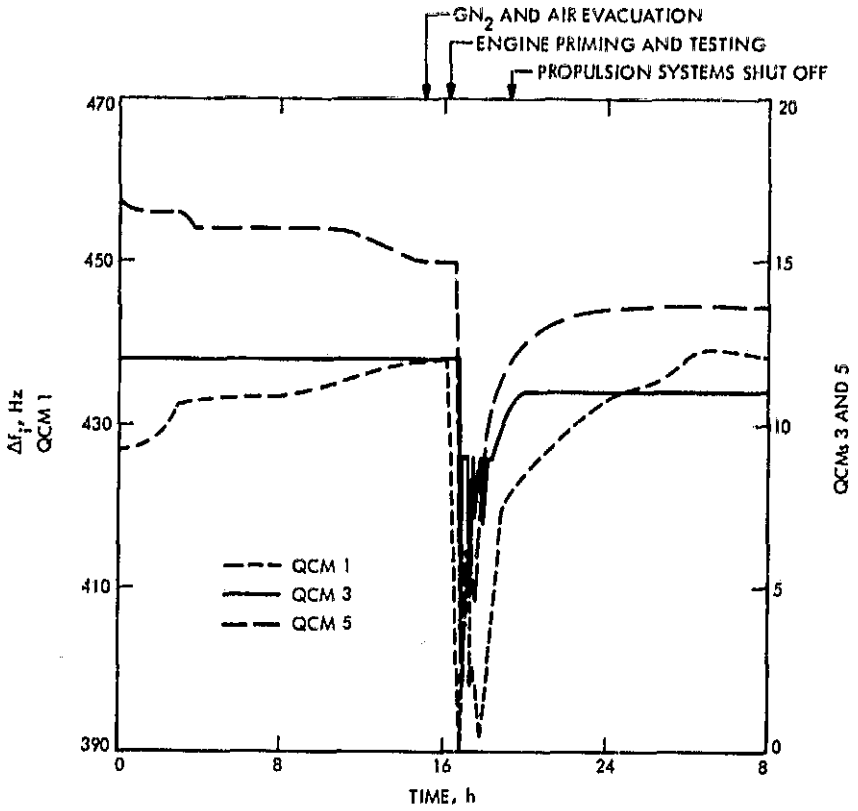

Fig. 28. Frequency variation of sun shield QCMs, August 15, 1972

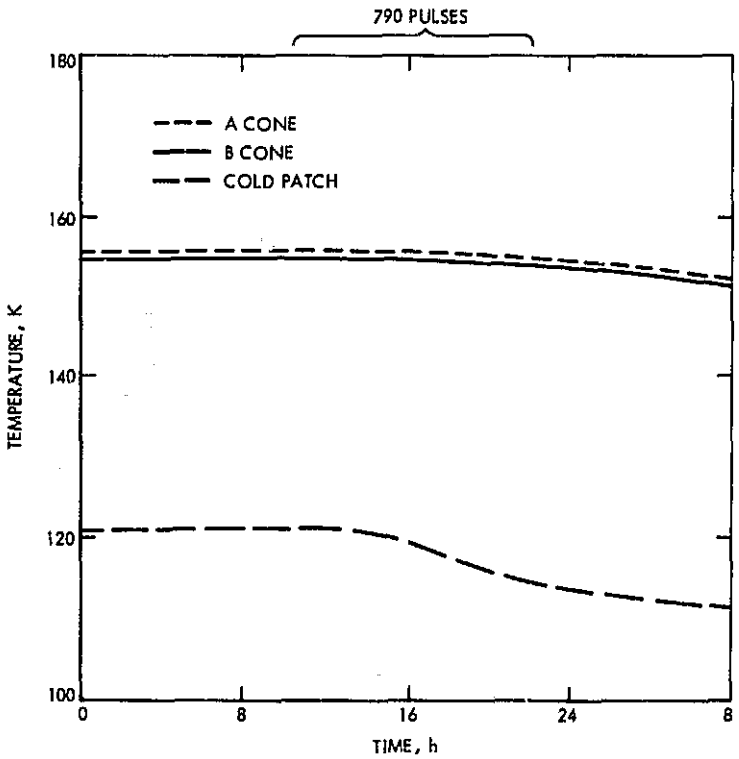

Fig. 29. Radiant cooler temperature variations, August 16, 1972

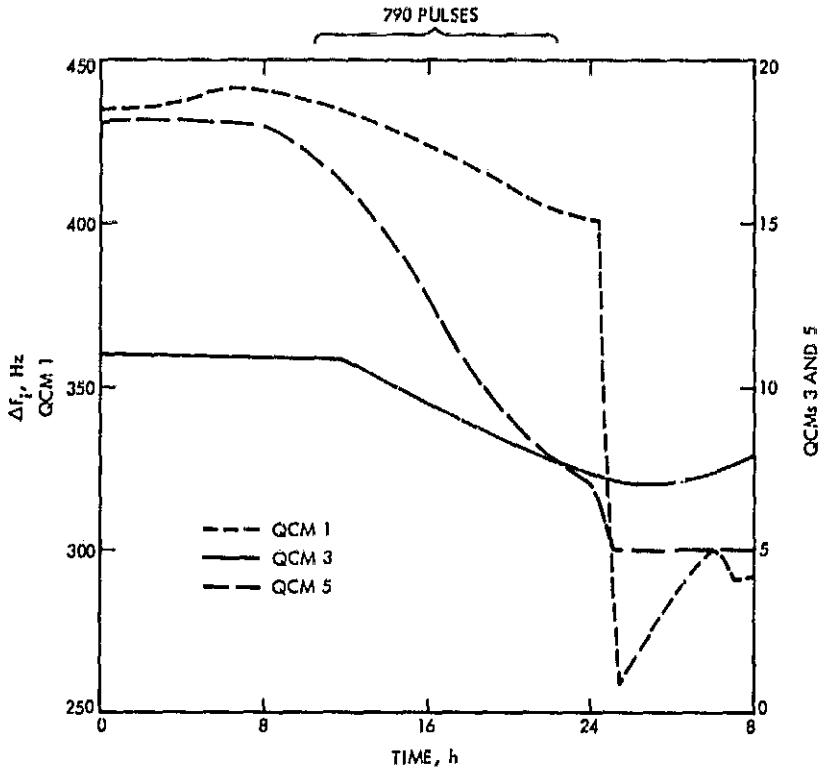

Fig. 30a. Frequency variation of sun shield QCMs, August 16, 1972

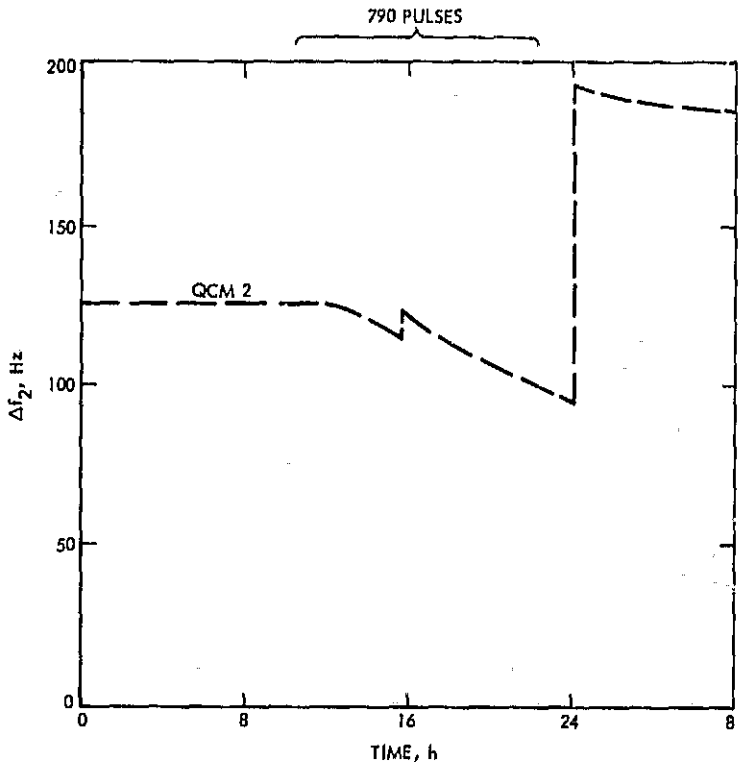

Fig. 30b. Frequency variation of radiant cooler QCM 2, August 16, 1972

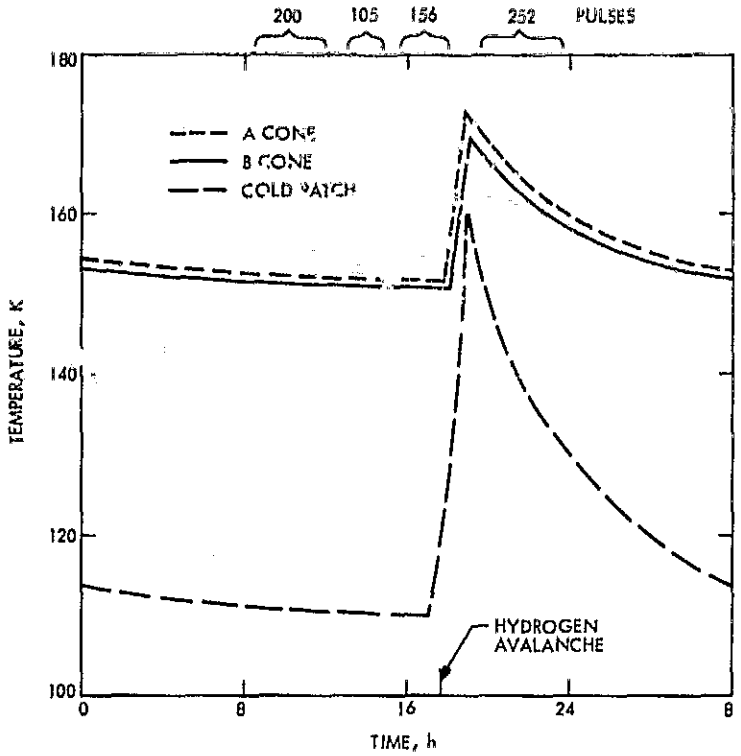

Fig. 31. Radiant cooler temperature variations, August 17, 1972

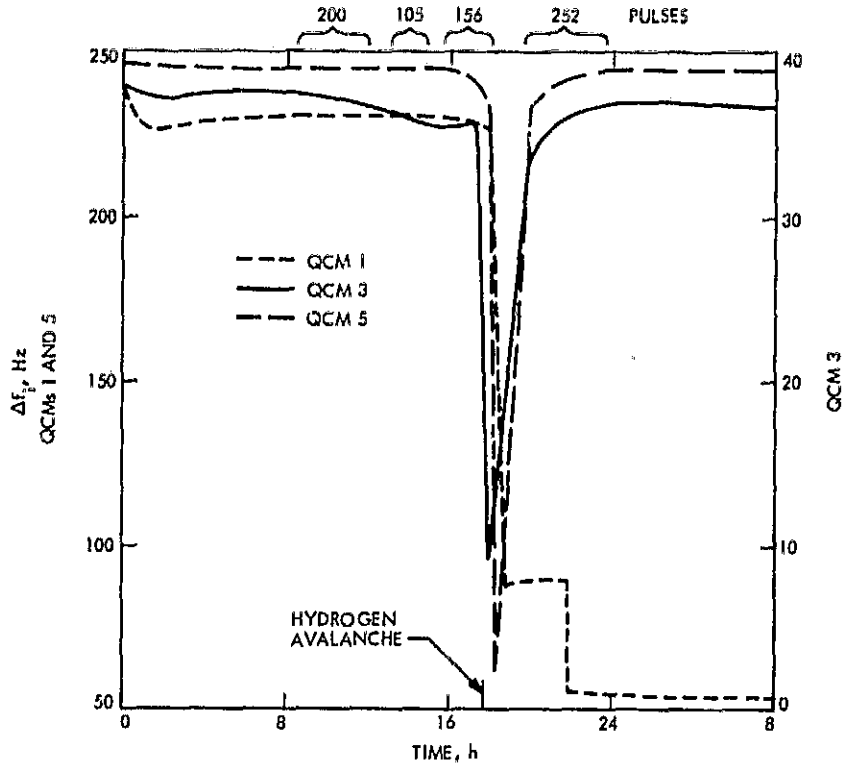

Fig. 32a. Frequency variation of sun shield QCMs, August 17, 1972

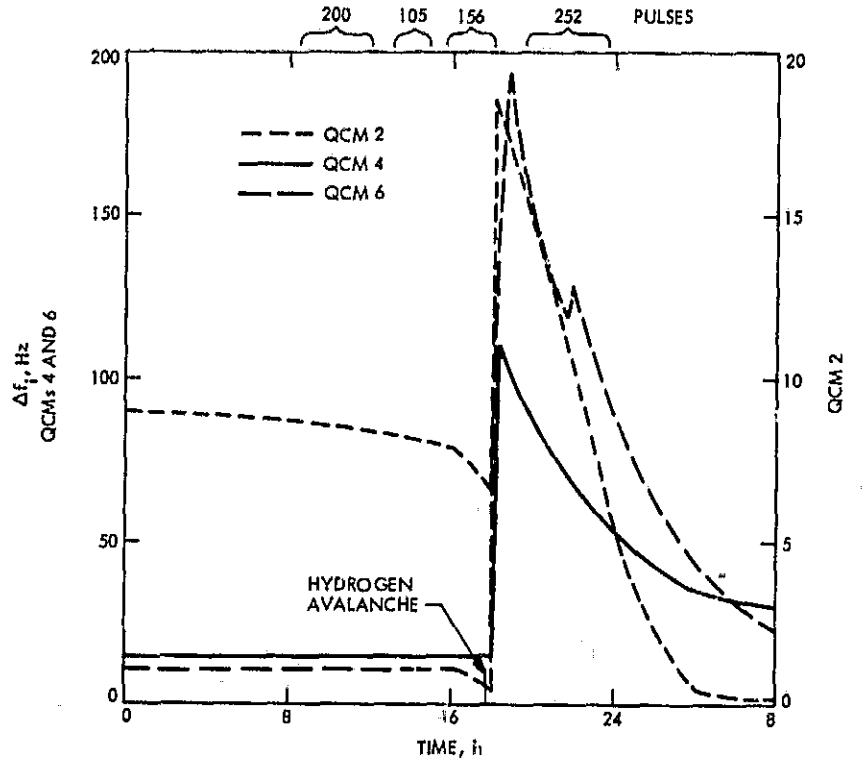

Fig. 32b. Frequency variation of radiant cooler QCMs, August 17, 1972

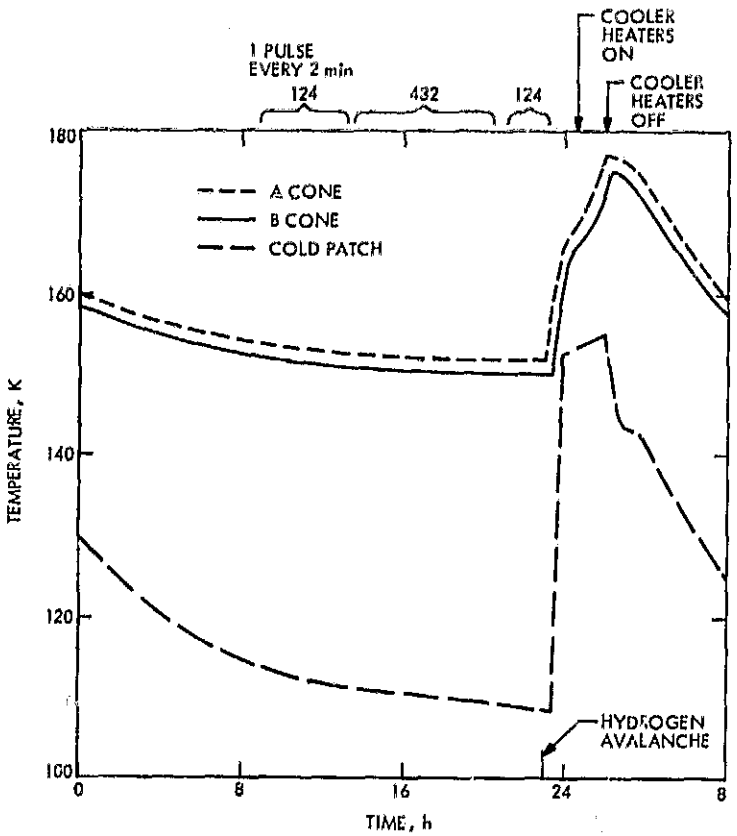

Fig. 33. Radiant cooler temperature variations, August 18, 1972

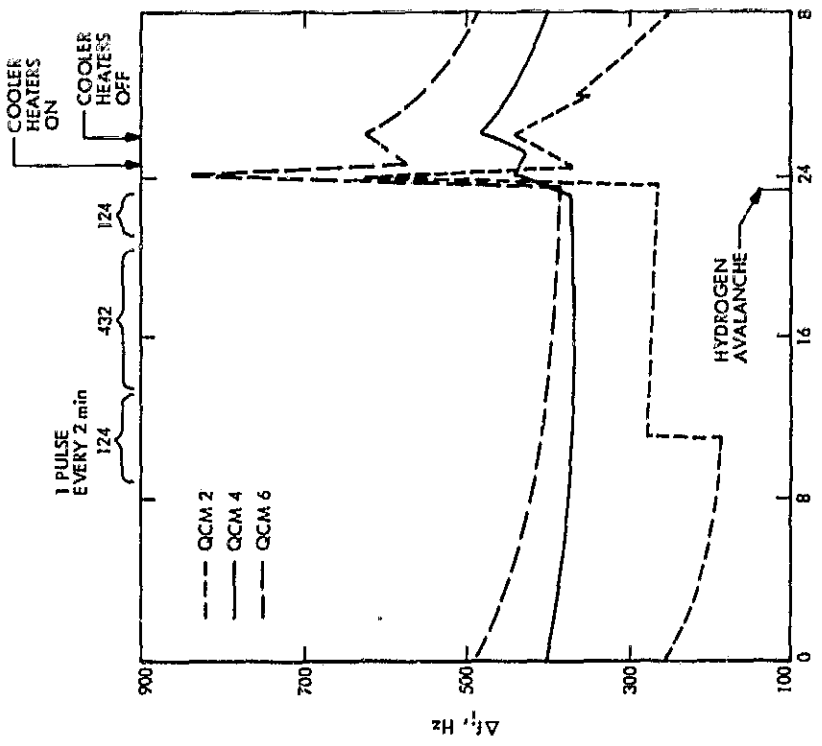

Fig. 34b. Frequency variation of radiant cooler QCMs, August 18, 1972

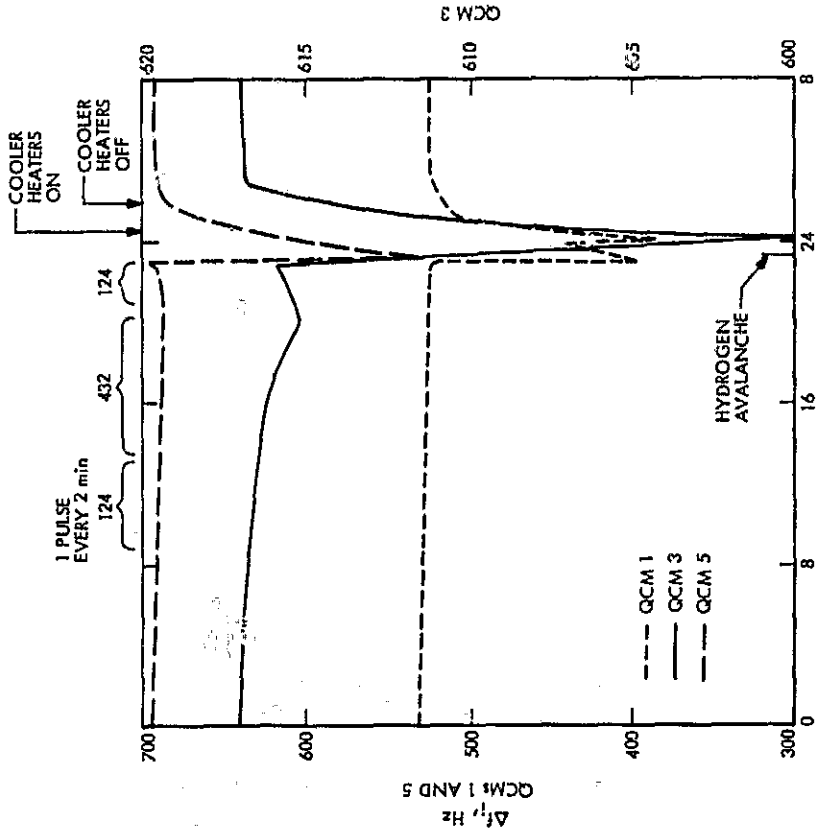

Fig. 34a. Frequency variation of sun shield QCMs, August 18, 1972

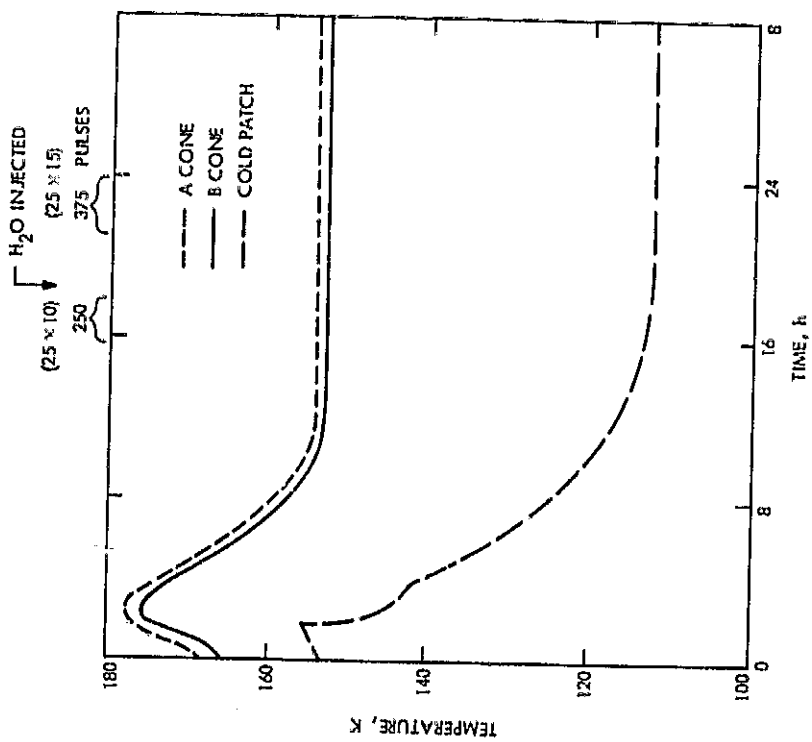

Fig. 35. Radiant cooler temperature variations, August 19, 1972

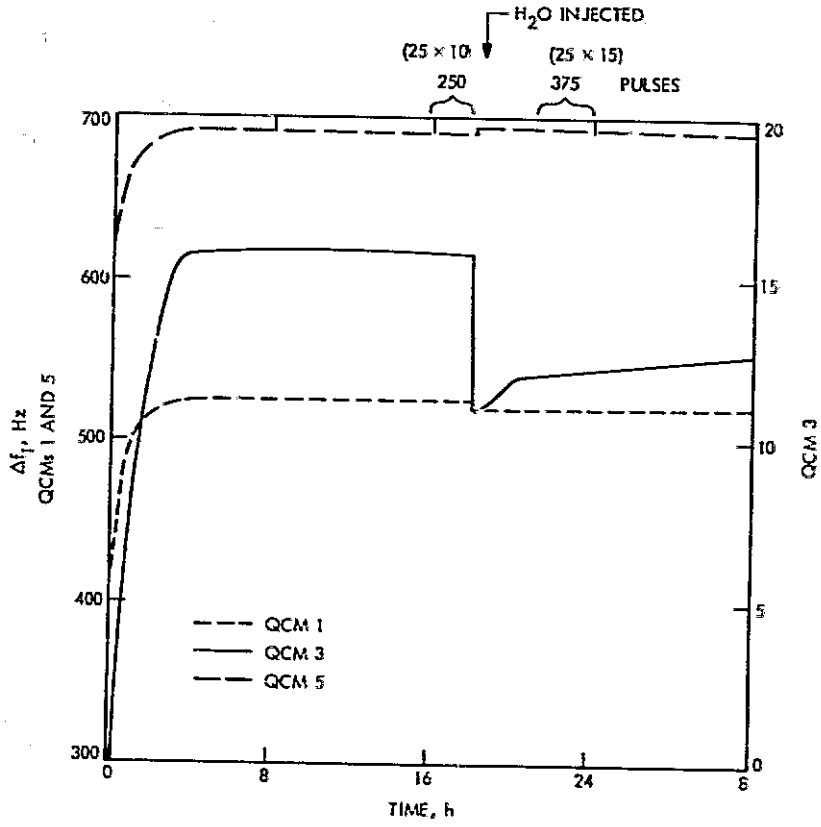

Fig. 36a. Frequency variation of sun shield QCMs, August 19, 1972

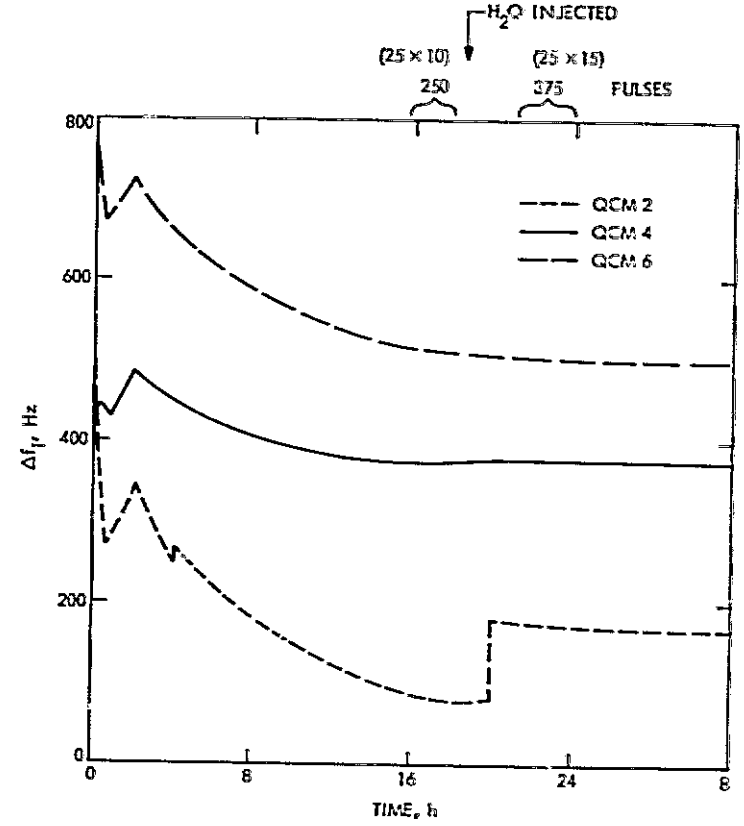

Fig. 36b. Frequency variation of radiant cooler QCMs, August 19, 1972

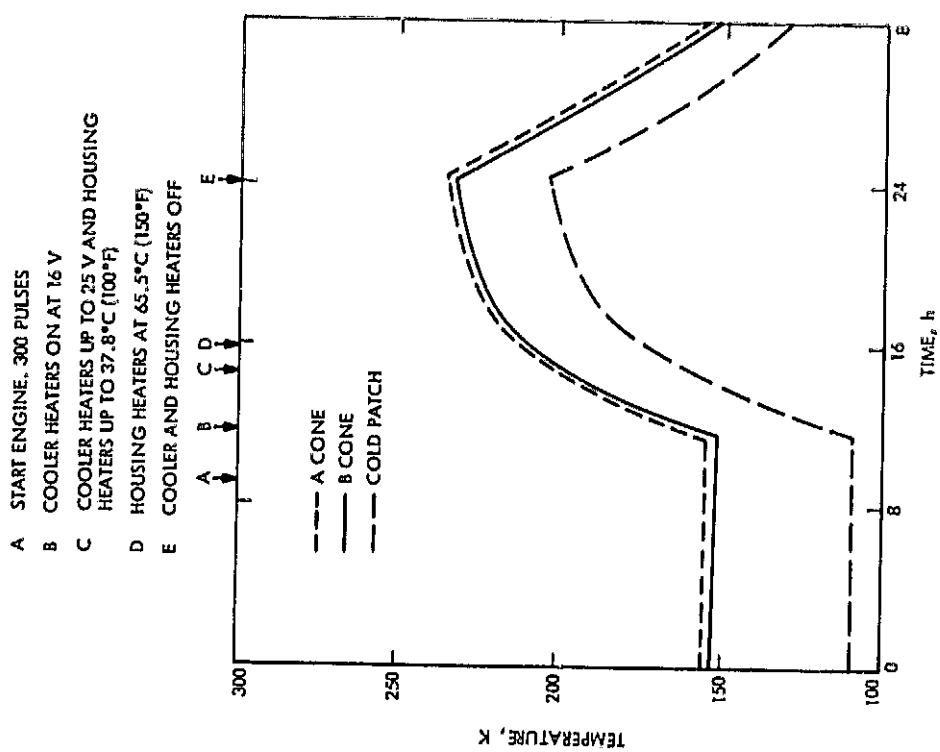

Fig. 37. Radiant cooler temperature variations, August 20, 1972

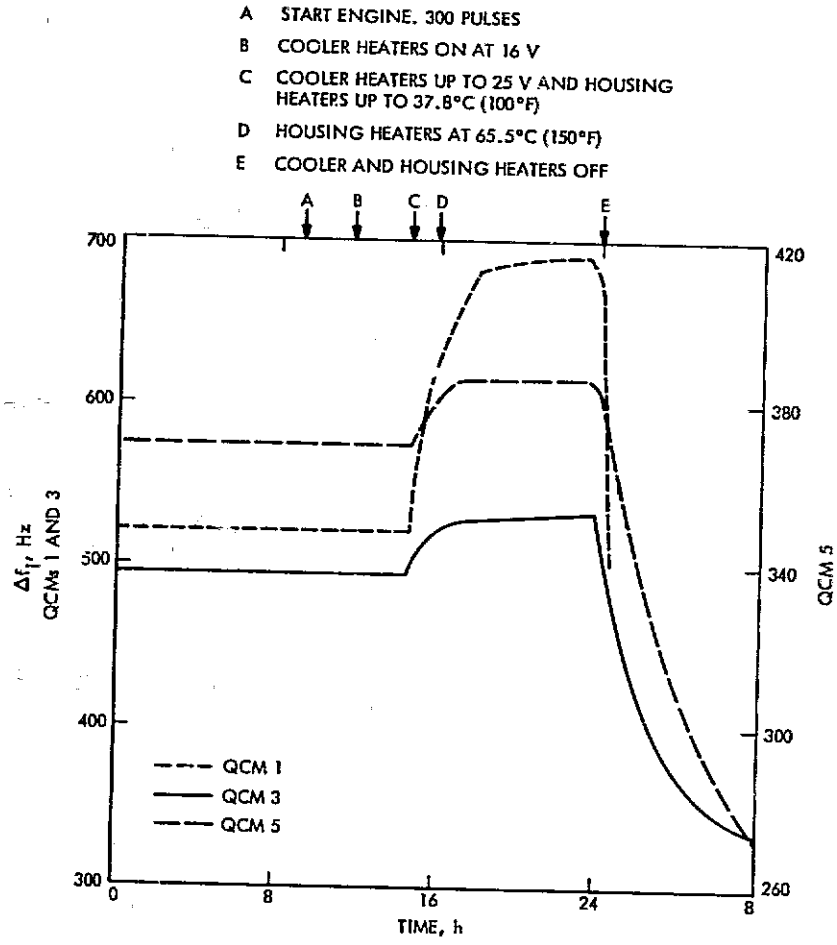

Fig. 38a. Frequency variation of sun shield QCMs, August 20, 1972

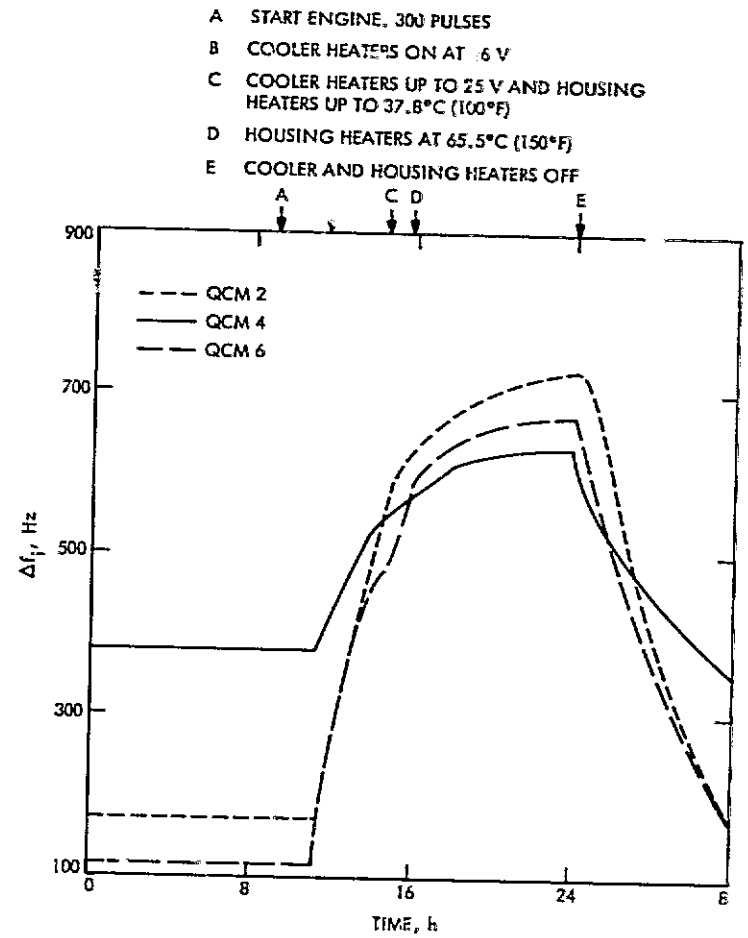

Fig. 38b. Frequency variation of radiant cooler QCMs, August 20, 1972

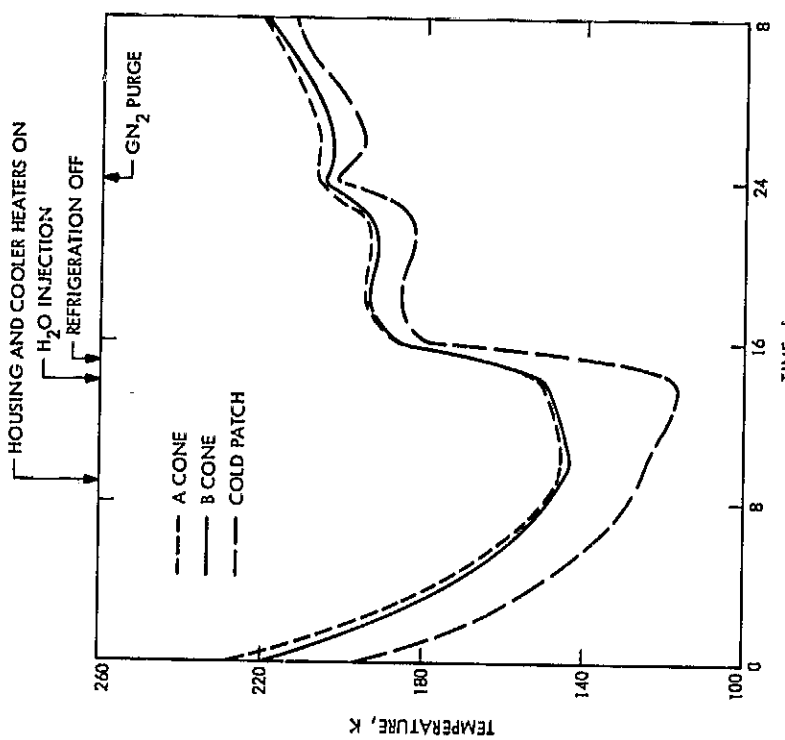

Fig. 39. Radiant cooler temperature variations, August 21, 1972

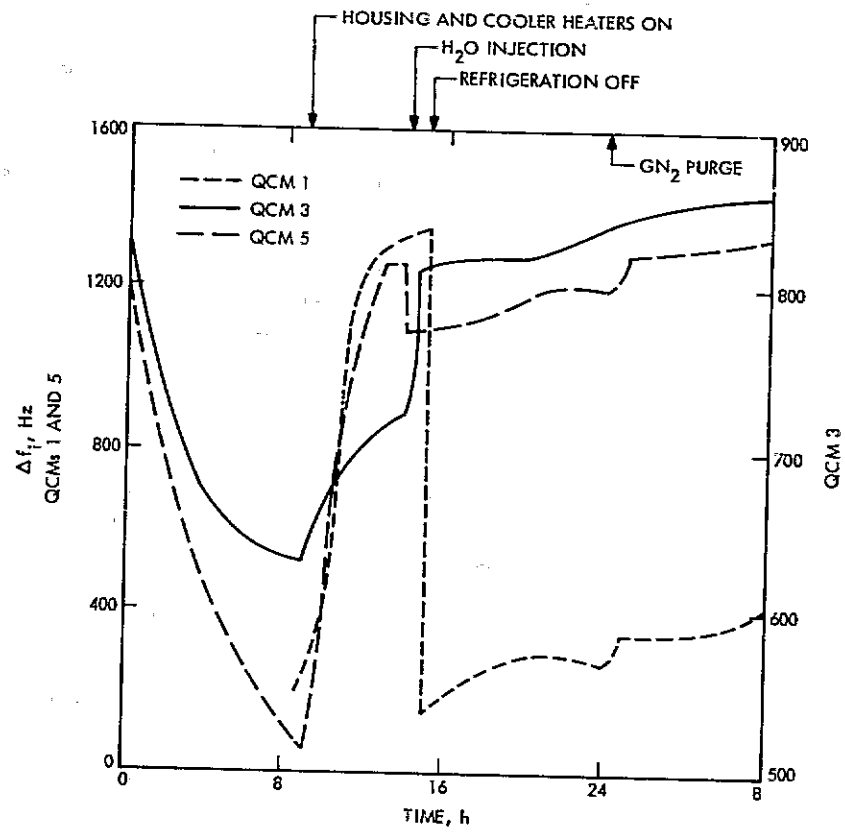

Fig. 40a. Frequency variation of sun shield QCMs, August 21, 1972

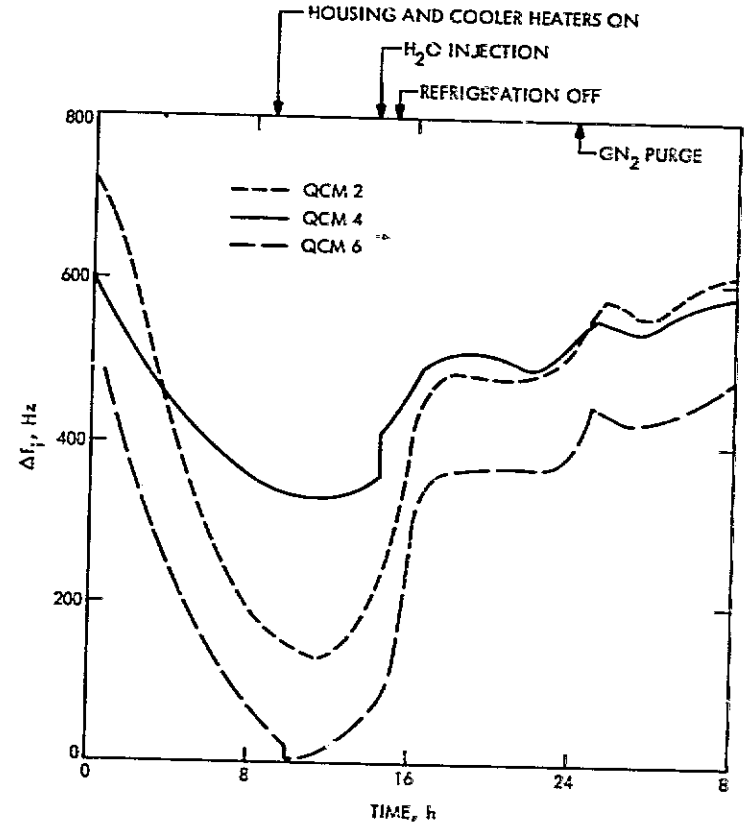

Fig. 40b. Frequency variation of radiant cooler QCMs, August 21, 1972

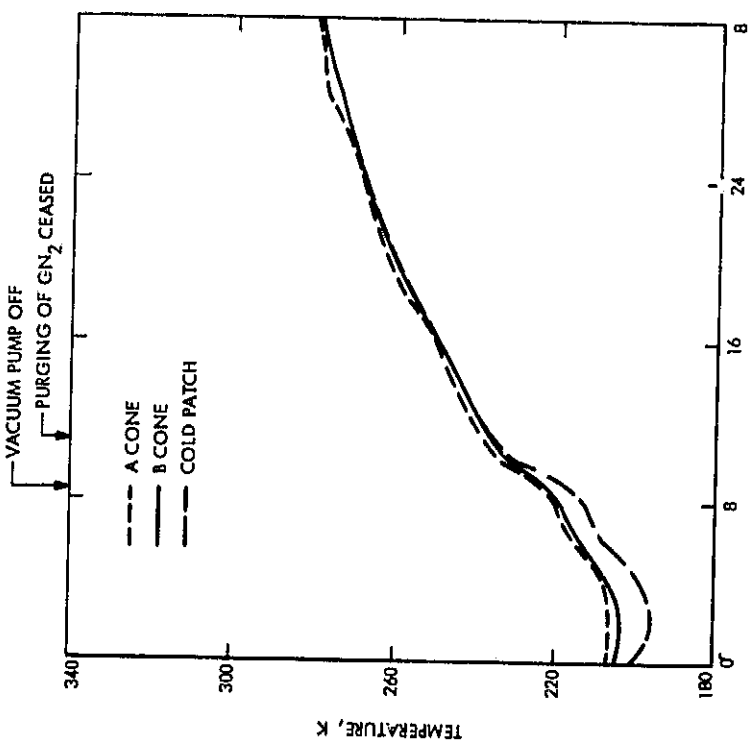

Fig. 41. Radiant cooler temperature variations, August 22, 1972

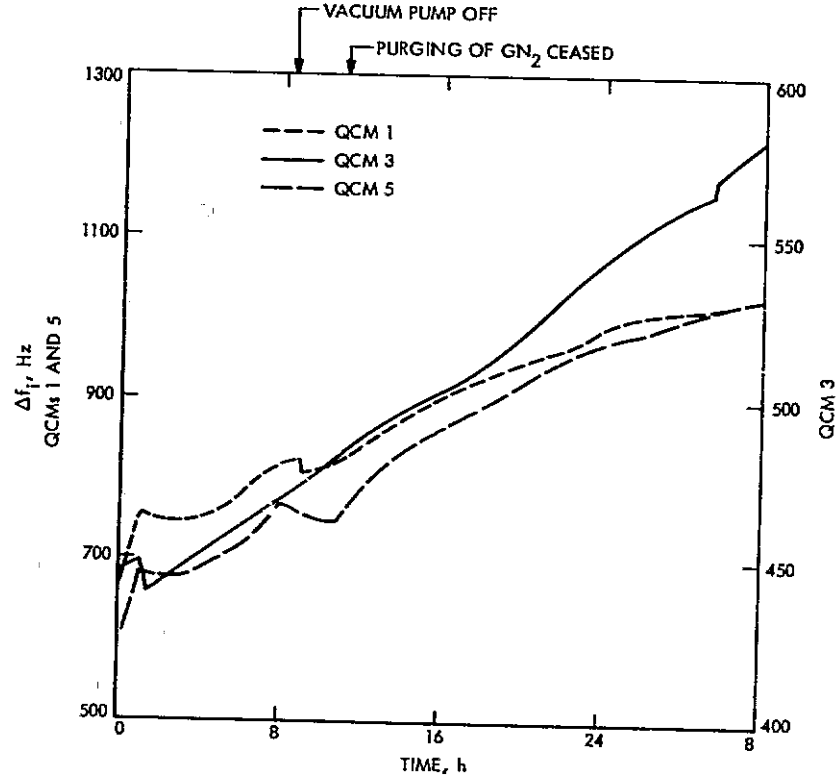

Fig. 42a. Frequency variation of sun shield QCMs, August 22, 1972

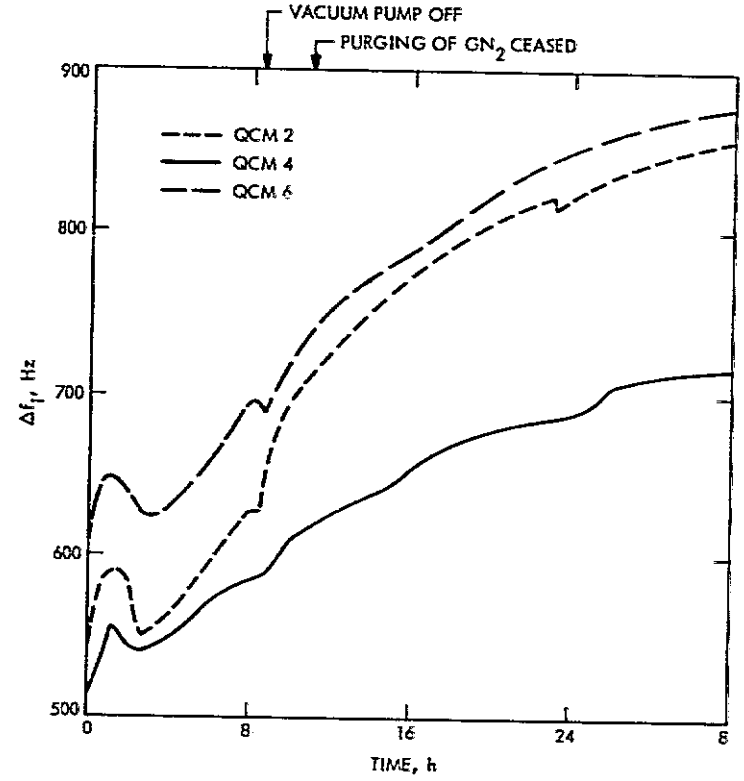

Fig. 42b. Frequency variation of radiant cooler QCMs, August 22, 1972

NASA — JPL — Coml., L.A., Calif.

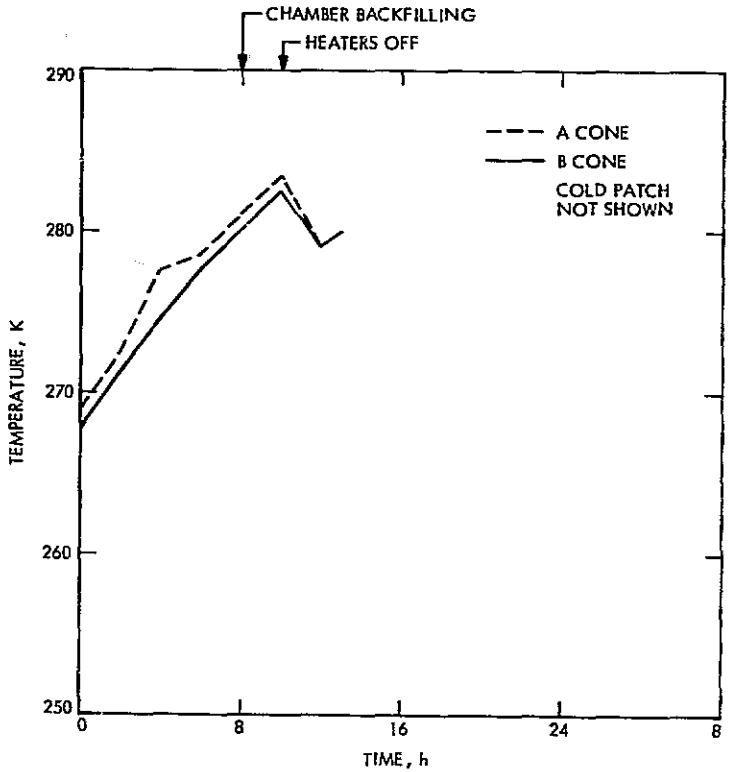

Fig. 43. Radiant cooler temperature variations, August 23, 1972

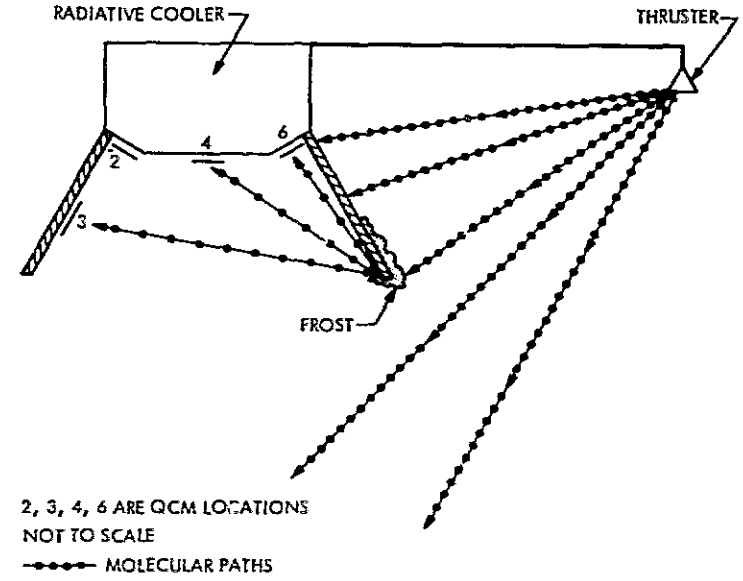

Fig. 44. Schematic representation of theorized frost formation on sun shield